

Maximal value for trilinear Higgs coupling in a 3-3-1 EFT

Adriano Cherchiglia ¹ and Leonardo J. Ferreira Leite ¹

¹*Instituto de Física Gleb Wataghin UNICAMP,
Rua Sérgio Buarque de Holanda, Campinas, SP, Brazil*

Recent efforts, both theoretical and experimental, have increasingly focused on the scalar potential of the Standard Model, with a highlight on the trilinear Higgs coupling. This parameter has long been recognized for its potential to test Beyond-Standard-Model (BSM) theories and its significance in understanding early cosmological dynamics. In order to broadly map BSM scenarios, a powerful tool is to devise its effective field theory (EFT) version for low-energies. In this work, we obtain a consistent EFT for a class of models based on the gauge group $SU(3)_c \times SU(3)_L \times U(1)_Y$. After properly matching the UV-complete theory at tree-level, we show that the EFT is a Two-Higgs-Doublet Model (2HDM), where some of the quartic couplings are naturally small. By imposing bounds from electroweak precision observables, collider, flavor, as well as theoretical considerations we obtain that the maximum value of the trilinear Higgs coupling is more than four times larger than the SM prediction, potentially testable at the LHC Hi-Lumi upgrade and other future colliders. Moreover, we find that such large values are only attainable if one considers an out-of-alignment scenario, even if the deviation is very small, which is not typically considered in the literature.

I. INTRODUCTION

One of the major achievements of the LHC experimental program was to find the last missing piece of the Standard Model (SM), the Higgs boson [1, 2]. After its discovery in 2012, a dedicated program started to assess if the scalar found by the LHC collaborations was indeed the one predicted by the SM. At present, its coupling to weak gauge bosons as well as third-generation fermions have been scrutinized, with excellent agreement [3, 4]. Soon, even the precision of its coupling to second generations fermions is expected to be increased. Even though the present scenario points to a scalar that behaves very SM-like, in particular regarding the Yukawa and kinetic Lagrangian, the scalar potential is known to a lesser extent. If the shape of the scalar potential presents deviations from the SM prediction, it could help to pave the way to Beyond Standard Model (BSM) scenarios, in particular in the case that no new mass resonances are found at the LHC. Particularly promising is the trilinear Higgs coupling λ_{hhh} , whose κ multiplier, $\kappa_\lambda = \lambda_{hhh}/(\lambda_{hhh})_{SM}$, is expected to be constrained to [0.5, 1.6] at 68% confidence-level in the LHC high-luminosity (HL-LHC) phase [5–7].

Knowledge of the scalar potential may also help to unveil mechanisms for baryogenesis, which typically requires the inclusion of extra scalars to the SM [8]. Some of the simplest extensions have been studied, where only scalar doublets and/or singlets are added, see [9, 10] for recent analysis, and [11] for a review. Regarding the 2HDM, even two-loop corrections to κ_λ are known [12–14]. Surprisingly, it was shown in [15] that the present knowledge of the trilinear Higgs coupling already restricts a region of the 2HDM parameter space allowed by all other relevant constraints. This conclusion relies on the inclusion of two-loop corrections, which can be up to 60% larger than the one-loop corrections for some corners of the parameter space.

The analysis for κ_λ in models with a more complex scalar sector is less explored. Among those, particularly interesting is the 3-3-1 model [16, 17], where the gauge group of the SM is extended to $SU(3)_C \otimes SU(3)_L \otimes U(1)_X$. Apart from providing an explanation for the number of families observed in Nature, it allows for a mechanism to generate neutrino masses and mixings [18–33], contain dark matter candidates [34–60], and address the strong CP problem [61–66]. By extending the gauge group, the 3-3-1 model contains a new set of gauge bosons, which have not been observed yet. Thus, the experimental collaborations can set lower bounds on their masses. For instance, the Z' mass has at

present a lower bound around 4 TeV [67]. In this scenario, it is natural to consider the case where the new gauge bosons have been integrated out, rendering an effective field theory (EFT). It was first argued in [68, 69], and further extended in [70], that the remaining particles, with masses at the electroweak scale, are the same as in the 2HDM [71]. In these analyses, however, it was only considered the case where the VEV of the first spontaneous symmetry breaking (from $SU(3)_C \otimes SU(3)_L \otimes U(1)_X$ to $SU(3)_C \otimes SU(2)_L \otimes U(1)_X$) was extremely large, decoupling entirely the extra gauge bosons (and some other scalars with masses also at this large scale). In the present work we provide a more consistent treatment of the underlying EFT, performing explicitly the matching between the 3-3-1 model and the 2HDM at tree-level. We will show that the scalar potential of 3-3-1 EFT can be entirely mapped into the most general 2HDM, with some of the quartic couplings being naturally suppressed. This will effectively render one-less free parameter for the 3-3-1 EFT, when compared not to the general 2HDM, but to the most studied scenario where a \mathbb{Z}_2 symmetry is imposed at one of the doublets. Moreover, regarding the Yukawa Lagrangian, since in the 3-3-1 model the quark families are not all in the same representation, it is not possible to couple all families of each quark type (down, up) to the same Higgs doublet. Thus, necessarily we have to treat one family distinctly, and the 3-3-1 EFT cannot be mapped to none of the usual four 2HDM types.

After properly defining the 3-3-1 EFT, we provide a comprehensive analysis regarding κ_λ , aiming to find its maximal value after imposing a set of experimental and theoretical bounds. Given that we have one-less parameter in comparison to the 2HDM, we will find a maximal value smaller than the one reported in [15]. Nevertheless, it can still be probed at the HL-LHC [5–7]. In the literature, it is generally assumed the exact alignment condition for the 2HDM, in order to avoid stringent constraints from colliders [72]. However, it is still possible to allow small deviations, which may open up a new region in parameter space particularly relevant for κ_λ . We have mapped the allowed region for 2HDM Type-I and Type-II as well as the 3-3-1 EFT, given present bounds. Given the relevance of this region, we also extended the analytic formulas for κ_λ at one-loop [12] for the non-alignment case. Extending the two-loop formula [13, 14] is beyond the scope of the present work. However, given its importance for the maximal allowed value of κ_λ in the strict alignment case [15], this enterprise may be particularly promising, which we leave for future investigation.

This work is organized as follows: in Section II we introduce the effective field description of the 3-3-1 model. In Section III we discuss the trilinear Higgs coupling (λ_{hhh}) in detail, comparing the differences expected from the 3-3-1 EFT and the 2HDM. Section IV is devoted to the description of phenomenological constraints our model is subjected to. We also perform the numerical evaluation of the available parameter space of our model, with emphasis on the maximum value allowed for the λ_{hhh} . We conclude in Section V. We provide two appendices. Appendix A contains a detailed analysis for κ_λ regarding 2HDM Types I and II, while Appendix B is related to the impact of including two-loop corrections for λ_{hhh} .

II. THE 3-3-1 EFT MODEL

The SM can be extended in a number of ways. The simplest proposal consists in the addition of new particles, grouped in irreducible representations of the SM gauge group. This approach is mainly guided by phenomenology, where some new phenomena (dark matter, neutrino masses and mixing, for instance) is explained due to the interaction of these new particles with themselves and at least some of their SM counterparts.

Another proposal consists in the modification of the SM gauge group. Models in this category usually replace the SM gauge group by one single, larger group, in the hope to provide a unification of the SM gauge couplings. In the same category, less ambitious models replace just one of the SM gauge sub-groups (or add new subgroups). The 3-3-1 model fits in this scenario, where the SM gauge group is replaced by $SU(3)_c \times SU(3)_L \times$

$U(1)_X$. In order to reproduce the SM particles and interactions, a set of electroweak symmetry breakings (EWSB) are proposed. We will consider a 3-3-1 version where only three scalar triplets η , ρ and χ are added, whose VEVs are responsible for the masses of gauge bosons as well as charged fermions. Complying with standard notation, the first breaking will be due to the VEV of χ , while the second breaking comes from the VEV of both η , ρ . Schematically,

$$SU(3)_C \otimes SU(3)_L \otimes U(1)_X \xrightarrow{v_\chi} SU(3)_C \otimes SU(2)_L \otimes U(1)_X \xrightarrow{v_\eta, v_\rho} SU(3)_C \otimes U(1)_{\text{em}}$$

In other to set our notation, we will choose the scalar triplets to have the following irreducible representation under the $SU(3)_c \times SU(3)_L \times U(1)_X$ gauge group

$$\eta = \begin{pmatrix} \eta^0 \\ \eta^- \\ \eta^{-A} \end{pmatrix} \sim (1, \mathbf{3}, X_\eta), \quad \rho = \begin{pmatrix} \rho^+ \\ \rho^0 \\ \rho^{-B} \end{pmatrix} \sim (1, \mathbf{3}, X_\rho), \quad \chi = \begin{pmatrix} \chi^A \\ \chi^B \\ \chi^0 \end{pmatrix} \sim (1, \mathbf{3}, X_\chi), \quad (1)$$

where the charges under $U(1)_X$ are given by

$$X_\eta = -\frac{1}{2} - \frac{\beta_Q}{2\sqrt{3}}, \quad X_\rho = \frac{1}{2} - \frac{\beta_Q}{2\sqrt{3}}, \quad X_\chi = \frac{\beta_Q}{\sqrt{3}} \quad (2)$$

Notice we have some freedom on the choice of the parameter β_Q . In terms of it, the electric charges of particles of type A or B are

$$Q^A = \frac{1}{2} + \frac{\sqrt{3}}{2}\beta_Q, \quad Q^B = -\frac{1}{2} + \frac{\sqrt{3}}{2}\beta_Q \quad (3)$$

In terms of the scalar triplets, the scalar potential takes the form

$$\begin{aligned} V(\eta, \rho, \chi) = & \mu_1^2 \rho^\dagger \rho + \mu_2^2 \eta^\dagger \eta + \mu_3^2 \chi^\dagger \chi + \lambda_1 (\rho^\dagger \rho)^2 + \lambda_2 (\eta^\dagger \eta)^2 + \lambda_3 (\chi^\dagger \chi)^2 \\ & + \lambda_{12} (\rho^\dagger \rho) (\eta^\dagger \eta) + \lambda_{13} (\chi^\dagger \chi) (\rho^\dagger \rho) + \lambda_{23} (\eta^\dagger \eta) (\chi^\dagger \chi) \\ & + \zeta_{12} (\rho^\dagger \eta) (\eta^\dagger \rho) + \zeta_{13} (\rho^\dagger \chi) (\chi^\dagger \rho) + \zeta_{23} (\eta^\dagger \chi) (\chi^\dagger \eta) \\ & - \sqrt{2} f \epsilon_{ijk} \eta_i \rho_j \chi_k + \text{h.c.}, \end{aligned} \quad (4)$$

In the equation above, we are implicitly assuming that $\beta_Q \neq \pm 1/\sqrt{3}$, otherwise terms with a odd number of fields would be present. Notice, however, that the case $\beta_Q = \pm 1/\sqrt{3}$ can still be considered if a \mathbb{Z}_2 symmetry (under which only χ is odd) is implicitly assumed¹. Once the χ^0 acquires a VEV, the remaining symmetry is $SU(3)_c \times SU(2)_L \times U(1)_Y$. At this stage, we can group the scalar fields in the following representations under the SM gauge group

$$\begin{aligned} \Phi_\eta = \begin{pmatrix} \eta^0 \\ -\eta^- \end{pmatrix} \sim (1, 2, -1/2), \quad \Phi_\rho = \begin{pmatrix} \rho^+ \\ \rho^0 \end{pmatrix} \sim (1, 2, 1/2), \quad \Phi_\chi = \begin{pmatrix} \chi^A \\ \chi^B \end{pmatrix} \sim (1, 2, \sqrt{3}\beta_Q/2) \\ \eta^{-A} \sim (1, 1, -Q^A), \quad \rho^{-B} \sim (1, 1, -Q^B), \quad \chi^0 \sim (1, 1, 0), \end{aligned} \quad (5)$$

while the scalar potential can be rewritten as

¹ The \mathbb{Z}_2 symmetry will be softly broken by the term $\sqrt{2} f \epsilon_{ijk} \eta_i \rho_j \chi_k$. If this term is discarded, one generates a massless CP-odd scalar, which is disfavoured by experiment.

$$\begin{aligned}
V(\eta, \rho, \chi) = & \mu_1^2(\Phi_\rho^\dagger\Phi_\rho + \rho^B\rho^{-B}) + \mu_2^2(\Phi_\eta^\dagger\Phi_\eta + \eta^A\eta^{-A}) + \mu_3^2(\chi^\dagger\chi) \\
& + \lambda_1(\Phi_\rho^\dagger\Phi_\rho + \rho^B\rho^{-B})^2 + \lambda_2(\Phi_\eta^\dagger\Phi_\eta + \eta^A\eta^{-A})^2 + \lambda_3(\chi^\dagger\chi)^2 \\
& + \lambda_{12}(\Phi_\rho^\dagger\Phi_\rho + \rho^B\rho^{-B})(\Phi_\eta^\dagger\Phi_\eta + \eta^A\eta^{-A}) \\
& + \lambda_{13}(\chi^\dagger\chi)(\Phi_\rho^\dagger\Phi_\rho + \rho^B\rho^{-B}) + \lambda_{23}(\Phi_\eta^\dagger\Phi_\eta + \eta^A\eta^{-A})(\chi^\dagger\chi) \\
& + \zeta_{12}(\Phi_\rho^\dagger\Phi_\eta + \rho^B\eta^{-A})(\Phi_\eta^\dagger\Phi_\rho + \eta^A\rho^{-B}) \\
& + \zeta_{13}(\Phi_\rho^\dagger\Phi_\chi + \rho^B\chi^0)(\Phi_\chi^\dagger\Phi_\rho + \chi^{0*}\rho^{-B}) \\
& + \zeta_{23}(\Phi_\eta^\dagger\Phi_\chi + \eta^A\chi^0)(\Phi_\chi^\dagger\Phi_\eta + \chi^{0*}\eta^{-A}) \\
& - \sqrt{2}f(\Phi_\eta^T\epsilon\Phi_\rho\chi^0 + \Phi_\rho^\dagger\Phi_\chi\rho^{-B} + \Phi_\eta^\dagger\Phi_\chi\eta^{-A} + \text{h.c.}). \tag{6}
\end{aligned}$$

At this stage, the scalar fields are not mass eigenstates in general. However, since we will assume the limit $v_\chi \gg v_\rho, v_\eta$, the mixing between χ_0 and the neutral components of $\Phi_{\rho,\eta}$ is suppressed [68, 69], rendering χ_0 a mass eigenstate. The fields η^A, ρ^B , on the other hand, are already mass eigenstates. As we are going to show, for all three fields (χ_0, η^A, ρ^B) their masses are proportional to v_χ in the limit $v_\chi \gg v_\rho, v_\eta$. Thus, these scalars can be considered heavy, in comparison to Φ_ρ, Φ_η , which will contain light fields. Defining $\langle\chi_0\rangle = v_\chi$ we obtain the tadpole equation

$$\frac{1}{v_\chi} \frac{\partial V}{\partial \chi_0} \Big|_{\chi_0=v_\chi} = 2\mu_3^2 + 4\lambda_3 v_\chi^2 \rightarrow \mu_3^2 = -2\lambda_3 v_\chi^2, \tag{7}$$

as well as the masses for the heavy fields (Φ_χ contains the Goldstones of the new gauge bosons)

$$m_{\chi_0}^2 = \frac{\partial^2 V}{\partial \chi_0^2} \Big|_{\chi_0=v_\chi} = 2\mu_3^2 + 12\lambda_3 v_\chi^2 = 8\lambda_3 v_\chi^2, \tag{8}$$

$$m_{\rho^B}^2 = \frac{\partial^2 V}{\partial \rho^B \rho^{-B}} \Big|_{\chi_0=v_\chi} = \mu_1^2 + \zeta_{13} v_\chi^2, \quad m_{\eta^A}^2 = \frac{\partial^2 V}{\partial \eta^A \eta^{-A}} \Big|_{\chi_0=v_\chi} = \mu_2^2 + \zeta_{23} v_\chi^2. \tag{9}$$

The parameters $\mu_{1,2}^2$ can be removed when considering the second gauge breaking. Nevertheless, since the scalar potential has only four dimensional parameters ($\mu_{1,2,3}^2$, and f), and after both breakings we have three VEVs, we can trade $\mu_{1,2,3}^2$ by the VEVs, in similarity to Eq. (7). It is easy to show that $\mu_{1,2}^2 \sim v_{\eta,\rho}^2$, implying that in the limit $v_\chi \gg v_\rho, v_\eta$, all heavy masses are proportional to v_χ , as previously stated.

In order to define a sensible effective field theory, we will integrate out the heavy fields χ, ρ_B, η_A . At tree-level matching, this can be conveniently done by solving the equation of motion (E.O.M.) for the heavy fields, defining our EFT Lagrangian. Notice that the fields $\Phi_\chi, \rho_B, \eta_A$ only appear in pairs in Eq. (4). Thus, considering tree-level matching, they can be integrated out without any consequence at low-energy. The only exception is for terms containing a single χ^0 , for instance $(\Phi_\eta^T\epsilon\Phi_\rho\chi^0)$, where there is just one heavy field coupled to light ones. Thus, as long as we consider only tree-level matching, terms of this kind are the only relevant. The EOM for χ_0 can be formally solved by

$$\chi_0 \approx \frac{\sqrt{2}f(\Phi_\eta^T\epsilon\Phi_\rho + \text{h.c.})}{m_{\chi_0}^2} - \frac{2\lambda_{13}v_\chi\Phi_\rho^\dagger\Phi_\rho}{m_{\chi_0}^2} - \frac{2\lambda_{23}v_\chi\Phi_\eta^\dagger\Phi_\eta}{m_{\chi_0}^2}, \tag{10}$$

where we are implicitly assuming that $f \ll v_\chi$. Finally, the scalar potential in the EFT, containing terms up to dimension 4, is given by

$$\begin{aligned}
V(\eta, \rho, \chi) = & (\mu_1^2 + \lambda_{13}v_\chi^2)(\Phi_\rho^\dagger\Phi_\rho) + (\mu_2^2 + \lambda_{23}v_\chi^2)(\Phi_\eta^\dagger\Phi_\eta) \\
& + \left[\lambda_1 - \frac{2v_\chi^2\lambda_{13}^2}{m_{\chi_0}^2} \right] (\Phi_\rho^\dagger\Phi_\rho)^2 + \left[\lambda_2 - \frac{2v_\chi^2\lambda_{23}^2}{m_\chi^2} \right] (\Phi_\eta^\dagger\Phi_\eta)^2 \\
& + \left[\lambda_{12} - \frac{4v_\chi^2\lambda_{13}\lambda_{23}}{m_{\chi_0}^2} \right] (\Phi_\rho^\dagger\Phi_\rho)(\Phi_\eta^\dagger\Phi_\eta) + \left[\zeta_{12} - \left(\frac{2f^2}{m_{\chi_0}^2} \right) \right] (\Phi_\eta^T \epsilon \Phi_\rho)^\dagger (\Phi_\eta^T \epsilon \Phi_\rho) \\
& + \left[-\sqrt{2}fv_\chi(\Phi_\eta^T \epsilon \Phi_\rho) - \left(\frac{f^2}{m_{\chi_0}^2} \right) (\Phi_\eta^T \epsilon \Phi_\rho)^2 + \left(\frac{2\sqrt{2}fv_\chi\lambda_{13}}{m_{\chi_0}^2} \right) (\Phi_\eta^T \epsilon \Phi_\rho) (\Phi_\rho^\dagger\Phi_\rho) \right. \\
& \left. + \left(\frac{2\sqrt{2}fv_\chi\lambda_{23}}{m_{\chi_0}^2} \right) (\Phi_\eta^\dagger\Phi_\eta) (\Phi_\eta^T \epsilon \Phi_\rho) + \text{h.c.} \right]. \tag{11}
\end{aligned}$$

It is immediate to notice that the above equation can be entirely mapped into the scalar potential of the 2HDM

$$\begin{aligned}
V(\Phi_1, \Phi_2) = & m_{11}^2\Phi_1^\dagger\Phi_1 + m_{22}^2\Phi_2^\dagger\Phi_2 + \frac{\Lambda_1}{2}(\Phi_1^\dagger\Phi_1)^2 + \frac{\Lambda_2}{2}(\Phi_2^\dagger\Phi_2)^2 \\
& + \Lambda_3(\Phi_1^\dagger\Phi_1)(\Phi_2^\dagger\Phi_2) + \Lambda_4(\Phi_1^\dagger\Phi_2)(\Phi_2^\dagger\Phi_1) + [-m_{12}^2\Phi_1^\dagger\Phi_2 \\
& + \frac{\Lambda_5}{2}(\Phi_1^\dagger\Phi_2)^2 + \Lambda_6(\Phi_1^\dagger\Phi_1)(\Phi_1^\dagger\Phi_2) + \Lambda_7(\Phi_2^\dagger\Phi_2)(\Phi_1^\dagger\Phi_2) + \text{h.c.}], \tag{12}
\end{aligned}$$

by performing the mapping $\Phi_\rho \rightarrow \Phi_1$ and $\Phi_\eta^C \rightarrow \Phi_2$.

Some comments are in order: when obtaining the masses of the scalars (in the limit $v_\chi \gg v_\rho, v_\eta$), one finds the relation $fv_\chi \sim m_A^2 s_\beta c_\beta$, where A is the pseudo-scalar and $\tan \beta = v_\eta/v_\rho$. Thus, the scale f is approximately given by $f \sim m_A^2/v_\chi$. By assuming that $m_A \ll v_\chi$, it is immediate to see that the 3-3-1 EFT scalar potential has Λ_5 suppressed. Another relation valid in the limit $v_\chi \gg v_\rho, v_\eta$ is $\lambda_{i3} \sim m_A^2/v_\chi^2$. Thus, we obtain that in the 3-3-1 EFT $\Lambda_{6,7}$ are also suppressed.

Up to this point, we only considered the scalar sector of the 3-3-1 when defining the 3-3-1 EFT. The influence of the heavy gauge sector can also be straightforwardly taken into account. It is achieved by resorting to the field Φ_χ , which contains the Goldstones of the extra gauge fields. As previously noticed, these fields only appear in pairs, together with η_A , and ρ_B . Thus, at tree-level matching, the heavy gauge fields leave no imprint in the low-energy scalars phenomenology. We proceed now to the Yukawa sector.

When defining the fermionic fields, we have some freedom regarding which of them will transform as (anti)triplets under the 3-3-1 gauge group. In order to easily map the third quark family to a type II 2HDM, we will adopt an opposite convention to the one employed in [70], as below

$$L_i = \begin{pmatrix} \nu_i \\ e_i \\ E_i \end{pmatrix}_L \sim \left(1, 3, -\frac{1}{2} - \frac{\beta_Q}{2\sqrt{3}} \right), \quad q_1 = \begin{pmatrix} d \\ -u \\ D \end{pmatrix}_L \sim \left(3, \bar{3}, \frac{1}{6} + \frac{\beta_Q}{2\sqrt{3}} \right), \tag{13}$$

$$q_2 = \begin{pmatrix} s \\ -c \\ S \end{pmatrix}_L \sim \left(3, \bar{3}, \frac{1}{6} + \frac{\beta_Q}{2\sqrt{3}} \right), \quad q_3 = \begin{pmatrix} t \\ b \\ T \end{pmatrix}_L \sim \left(3, 3, \frac{1}{6} - \frac{\beta_Q}{2\sqrt{3}} \right), \tag{14}$$

$$u_R, c_R, t_R \sim (3, 1, 2/3) \quad d_R, s_R, b_R \sim (3, 1, -1/3), \quad e_R \sim (1, 1, -1), \tag{15}$$

$$D_R, S_R \sim \left(3, 1, \frac{1}{6} + \frac{\sqrt{3}\beta_Q}{2} \right), \quad T_R \sim \left(3, 1, \frac{1}{6} - \frac{\sqrt{3}\beta_Q}{2} \right), \quad E_R \sim \left(1, 1, -\frac{1}{2} - \frac{\sqrt{3}\beta_Q}{2} \right) \tag{16}$$

The electric charges of the D, S, T fields (both left and right-handed) are given by

$$Q_{E_i} = -\frac{1}{2} + \frac{\sqrt{3}\beta_Q}{2} \quad Q_{D,S} = \frac{1}{6} - \frac{\sqrt{3}\beta_Q}{2} \quad Q_T = \frac{1}{6} + \frac{\sqrt{3}\beta_Q}{2} \tag{17}$$

Under the 3-3-1 gauge group, we can write the Yukawa lagrangian as below²

$$-\mathcal{L}_{\text{Yuk}}^q = y_{ij}^u \bar{q}_{iL} \rho^* u_{jR} + y_{3j}^u \bar{q}_{3L} \eta u_{jR} + y_{ij}^d \bar{q}_{iL} \eta^* d_{jR} + y_{3j}^d \bar{q}_{3L} \rho d_{jR} \\ + y_i^D \bar{q}_{iL} \chi^* D_R + y_i^S \bar{q}_{iL} \chi^* S_R + y^T \bar{q}_{3L} \chi T_R + \text{h.c.} \quad (18)$$

$$-\mathcal{L}_{\text{Yuk}}^l = y_{mn}^e \bar{L}_{mL} \rho e_{nR} + y_{mn}^E \bar{L}_{mL} \chi E_{nR} + \text{h.c.} \quad (19)$$

where $i = \{1, 2\}$, while the other indexes go from 1 to 3. Notice that we are singling out the third family quarks, choosing them to be components of a triplet (see, for instance [73] for other possibilities). After the first gauge breaking, we obtain

$$-\mathcal{L}_{\text{Yuk}}^q = y_{ij}^u \bar{q}_{iL} \Phi_\rho^* u_{jR} + y_{1j}^u \bar{D}_L \rho^B u_{jR} + y_{2j}^u \bar{S}_L \rho^B u_{jR} + y_{3j}^u \bar{q}_{3L} \Phi_\eta u_{jR} + y_{3j}^u \bar{T}_L \eta^{-A} u_{jR} \\ + y_{ij}^d \bar{q}_{iL} \Phi_\eta^* d_{jR} + y_{1j}^d \bar{D}_L \eta^A d_{jR} + y_{2j}^d \bar{S}_L \eta^A d_{jR} + y_{3j}^d \bar{q}_{3L} \Phi_\rho d_{jR} + y_{3j}^d \bar{T}_L \rho^{-B} d_{jR} \\ + y_1^D \bar{D}_L \chi_0^* D_R + y_2^D \bar{S}_L \chi_0^* D_R + y_1^S \bar{D}_L \chi_0^* S_R + y_2^S \bar{S}_L \chi_0^* S_R + y^T \bar{T}_L \chi_0 T_R \\ + v_\chi y_1^D \bar{D}_L D_R + v_\chi y_2^D \bar{S}_L D_R + v_\chi y_1^S \bar{D}_L S_R + v_\chi y_2^S \bar{S}_L S_R + v_\chi y^T \bar{T}_L T_R + \text{h.c.} \quad (20)$$

$$-\mathcal{L}_{\text{Yuk}}^l = y_{mn}^e \bar{l}_{mL} \Phi_\rho e_{nR} + y_{mn}^e \bar{E}_{mL} \rho^{-B} e_{nR} + y_{mn}^E \bar{E}_{mL} \chi_0 E_{nR} + v_\chi y_{mn}^E \bar{E}_{mL} E_{nR} + \text{h.c.} \quad (21)$$

Considering that the yukawas (y^D, y^S, y^T, y^E) are order 1, the masses of the extra fermions will be around the scale v_χ , which is heavy. Thus, we can also integrate them from our theory. Notice, however, that most terms contain a even number of heavy fields, the only exception is the ones containing χ_0 , which is odd but contain three heavy fields. Therefore, we can only have corrections at one-loop matching, and the 3-3-1 EFT Yukawa sector is simply given by

$$-\mathcal{L}_{\text{Yuk}}^q = y_{1j}^u (\bar{d}_L \rho^- - \bar{u}_L \rho^0) u_{jR} + y_{2j}^u (\bar{s}_L \rho^- - \bar{c}_L \rho^0) u_{jR} + y_{3j}^u (\bar{t}_L \eta^0 - \bar{b}_L \eta^-) u_{jR} \\ + y_{1j}^d (\bar{u}_L \eta^+ + \bar{d}_L \eta^0) d_{jR} + y_{2j}^d (\bar{c}_L \eta^+ + \bar{s}_L \eta^0) d_{jR} + y_{3j}^d (\bar{b}_L \rho^0 + \bar{t}_L \rho^+) d_{jR} + \text{h.c.} \quad (22)$$

$$-\mathcal{L}_{\text{Yuk}}^l = y_{mn}^e (\bar{e}_{mL} \rho^0 + \bar{\nu}_{mL} \rho^+) e_{nR} + \text{h.c.} \quad (23)$$

Resorting, for simplicity, to a third family only case we obtain

$$-\mathcal{L}_{\text{Yuk}}^q \supset y_{33}^u (\bar{t}_L \eta^0 - \bar{b}_L \eta^-) t_R + y_{33}^d (\bar{b}_L \rho^0 + \bar{t}_L \rho^+) b_R + \text{h.c.} \quad (24)$$

$$-\mathcal{L}_{\text{Yuk}}^l \supset y_{33}^e (\bar{\tau}_L \rho^0 + \bar{\nu}_{\tau L} \rho^+) \tau_R + \text{h.c.} \quad (25)$$

Notice that the tau as well as the bottom will receive their masses through v_ρ , while the top mass comes from v_η . Recalling that $\tan \beta = v_\eta/v_\rho$, it is clear that $y_{33}^u = (m_t/v)(\sqrt{2}/s_\beta)$, while $y_{33}^d = (m_b/v)(\sqrt{2}/c_\beta)$, $y_{33}^e = (m_\tau/v)(\sqrt{2}/c_\beta)$ where $v = \sqrt{v_\eta^2 + v_\rho^2} = 246$ GeV. Requiring perturbativity of the Yukawa couplings, it follows that $\tan \beta$ must be larger than unity. Moreover, the pattern for the couplings between the fermions and the scalars mimics the one found in the Type II 2HDM. Thus, as long as we focus only on the third family fermions, the 3-3-1 EFT Yukawa sector can be mapped to the Type II 2HDM.

III. THE TRILINEAR HIGGS COUPLING

One of the main results of our contribution is to unveil the maximum allowed value for the trilinear Higgs coupling (λ_{hhh}) in the context of the 3-3-1 EFT. Before delving

² For the choice $\beta_Q = \pm 1/\sqrt{3}$, we will consider the fields D_R, S_R, T_R , and E_R to be odd under the \mathbb{Z}_2 introduced for this case.

into this task, we will present the analytical formula for such quantity in the 2HDM up to one-loop order. At tree-level, we obtain [74]

$$\lambda_{hhh}^{(0)} = -\frac{3m_h^2}{2vs_{2\beta}} \left[\cos(3\alpha - \beta) + 3\cos(\alpha + \beta) - 4\cos^2(\alpha - \beta)\cos(\alpha + \beta)\frac{M^2}{m_h^2} \right], \quad (26)$$

where $M^2 = m_{12}^2/s_\beta c_\beta$, and we have the tree-level relation

$$M^2 = m_A^2 + \lambda_5 v^2 + \frac{1}{2}\lambda_6 t_\beta^{-1} + \frac{1}{2}\lambda_7 t_\beta. \quad (27)$$

The result in the SM is obtained in the alignment limit where $\sin(\beta - \alpha) = 1$,

$$(\lambda_{hhh})_{SM} = -\frac{3m_h^2}{v}. \quad (28)$$

It allows to define the κ multiplier

$$\kappa_\lambda = \frac{\lambda_{hhh}}{(\lambda_{hhh})_{SM}}, \quad (29)$$

which we will use hereafter. Before proceeding to the one-loop expression, it will be useful to have the tree-level expression close to the alignment limit. Using that $\sin(\beta - \alpha) = \sin(\pi/2 + x) = \cos(x) \sim 1 - x^2/2$, we obtain

$$\kappa_\lambda^{(0)} = 1 + \frac{3}{2}x^2 - 2x^3 \cot(2\beta) - \frac{13x^4}{8} - \left(2x^2 - 2x^3 \cot(2\beta) - \frac{5x^4}{3} \right) \frac{M^2}{m_h^2} \quad (30)$$

We notice that, from $\mathcal{O}(x^3)$, there is a dependence on $\tan\beta$. At loop order, considering terms up to $\mathcal{O}(x^2)$ as well as loops containing either BSM particles or the top, we obtain [12]

$$\begin{aligned} \kappa_\lambda^{2\text{HDM}} = & 1 + \frac{3}{2} \left(1 - \frac{4M^2}{3m_h^2} \right) x^2 + \frac{m_H^4}{12\pi^2 m_h^2 v^2} \left(1 - \frac{M^2}{m_H^2} \right)^3 + \frac{m_A^4}{12\pi^2 m_h^2 v^2} \left(1 - \frac{M^2}{m_A^2} \right)^3 \\ & + \frac{m_{H^\pm}^4}{6\pi^2 m_h^2 v^2} \left(1 - \frac{M^2}{m_{H^\pm}^2} \right)^3 - \frac{m_t^4}{\pi^2 m_h^2 v^2} \end{aligned} \quad (31)$$

Notice that the top contribution decreases κ_λ . It is also clear that κ_λ deviates from unity for large splitting between M and the BSM scalars. In the 2HDM in general, M can be chosen as a free parameter, so one has the freedom to maximize κ_λ by a suitable adjustment of M (in particular, by adopting a large splitting between M and the BSM scalar masses). In the 3-3-1 EFT it is no longer allowed, since M is given by

$$\begin{aligned} M^2 = & m_A^2 + \lambda_5 v^2 + \frac{1}{2}\lambda_6 t_\beta^{-1} + \frac{1}{2}\lambda_7 t_\beta \\ \sim & m_A^2 - \left(\frac{f^2}{m_{\chi_0}^2} \right) v^2 + \frac{1}{2} \left(\frac{2\sqrt{2}f v_\chi \lambda_{13}}{m_{\chi_0}^2} \right) t_\beta^{-1} + \frac{1}{2} \left(\frac{2\sqrt{2}f v_\chi \lambda_{23}}{m_{\chi_0}^2} \right) t_\beta \end{aligned} \quad (32)$$

where $m_A^2 = \frac{fv_\chi}{c_\beta s_\beta} + \frac{fv^2 c_\beta s_\beta}{v_\chi} \sim \frac{fv_\chi}{c_\beta s_\beta}$. We are interested in the regime where m_A is relatively light (up to TeV), while $v_\chi \gg v$. Therefore, we are required to choose $f \ll v_\chi$. Since the 3-3-1 EFT is defined in the regime that $m_{\chi_0} \sim v_\chi$ we obtain that $M^2 \sim m_A^2$, implying

$$\begin{aligned} \kappa_\lambda^{331} \sim & 1 + \frac{3}{2} \left(1 - \frac{4m_A^2}{3m_h^2} \right) x^2 - \frac{m_t^4}{\pi^2 m_h^2 v^2} + \frac{m_H^4}{12\pi^2 m_h^2 v^2} \left(1 - \frac{m_A^2}{m_H^2} \right)^3 \\ & + \frac{m_{H^\pm}^4}{6\pi^2 m_h^2 v^2} \left(1 - \frac{m_A^2}{m_{H^\pm}^2} \right)^3 \end{aligned} \quad (33)$$

The formula above provides a good approximation for κ_λ as we are going to show in the end of the section. It can be compared against the prediction obtained from *anyH3*, a package to compute λ_{hhh} up to one-loop in general BSM models [75]. We will, however, include some refinements of the formula above. First, in the 2HDM, the normalized top Yukawa is given by

$$\xi_u = \left(\frac{\cos(\beta - \alpha)}{\tan\beta} + \sin(\beta - \alpha) \right) \quad (34)$$

Also, following [76], in the SM case there are sub-leading contributions from the top, as well as loop corrections containing the SM Higgs

$$\lambda_{hhh}^{sub} = -\frac{3m_h^2}{v} \left\{ \frac{m_h^2}{2\pi^2 v^2} + \frac{7m_t^2}{32\pi^2 v^2} \right\} \quad (35)$$

Moreover, as we deviate from the alignment limit, there are corrections from the other trilinear scalar couplings, which appear in triangle diagrams containing BSM scalars. Since these couplings are behind the appearance of the factors $\left(1 - \frac{M^2}{m_{\text{BSM}}^2}\right)^3$ in Eq. (31), we can just adapt them from the general non-alignment case. By inspection of the scalar couplings in the 2HDM, we will perform the replacements

$$\left(1 - \frac{M^2}{m_A^2}\right) \rightarrow \left(1 - \frac{M^2}{m_A^2}\right) + \frac{M^2 - m_h^2}{2m_A^2} \left(t_\beta - \frac{1}{t_\beta}\right) x \quad (36)$$

$$\left(1 - \frac{M^2}{m_{H^\pm}^2}\right) \rightarrow \left(1 - \frac{M^2}{m_{H^\pm}^2}\right) + \frac{M^2 - m_h^2}{2m_{H^\pm}^2} \left(t_\beta - \frac{1}{t_\beta}\right) x \quad (37)$$

$$\left(1 - \frac{M^2}{m_H^2}\right) \rightarrow \left(1 - \frac{M^2}{m_H^2}\right) - \frac{2m_H^2 + m_h^2 - 3M^2}{2m_H^2} \left(t_\beta - \frac{1}{t_\beta}\right) x \quad (38)$$

Finally, the κ_λ^{331} , including the sub-leading corrections and keeping terms up to $\mathcal{O}(x^3)$ will be given by

$$\begin{aligned} \kappa_\lambda^{331} \sim & 1 + \frac{3}{2} \left(1 - \frac{4m_A^2}{3m_h^2}\right) x^2 + \frac{m_A^2 - m_h^2}{m_h^2} \left(t_\beta - \frac{1}{t_\beta}\right) x^3 - \frac{m_t^4}{\pi^2 m_h^2 v^2} \left(1 - \frac{7m_h^2}{32m_t^2}\right) \xi_u^3 \\ & + \frac{m_h^2}{2\pi^2 v^2} + \frac{m_H^4}{12\pi^2 m_h^2 v^2} \left[1 - \frac{m_A^2}{m_H^2} + \frac{2m_H^2 + m_h^2 - 3m_A^2}{2m_H^2} \left(t_\beta - \frac{1}{t_\beta}\right) x\right]^3 \\ & + \frac{m_{H^\pm}^4}{6\pi^2 m_h^2 v^2} \left[1 - \frac{m_A^2}{m_{H^\pm}^2} + \frac{m_A^2 - m_h^2}{2m_{H^\pm}^2} \left(t_\beta - \frac{1}{t_\beta}\right) x\right]^3 + \frac{(m_A^2 - m_h^2)^3 x^3}{96\pi^2 m_h^2 m_A^2 v^2} \left(t_\beta - \frac{1}{t_\beta}\right)^3 \end{aligned} \quad (39)$$

In the remaining of the section, we discuss the agreement between the last formula (for 3-3-1 EFT as well general 2HDM) and the full calculation obtained by employing *anyH3* [75]. We include in the legends of the following figures if we are considering the 2HDM in general (for which M is as free parameter) or the 3-3-1 EFT. In Fig. 1 we show the difference between the approximate ($\bar{\kappa}_\lambda$) and the full formula (κ_λ), in terms of the SM Higgs mass. Since we are considering the alignment limit ($s_{\beta-\alpha} = 1$), and degenerate masses, we recover the SM result. Notice the importance of the sub-leading correction due to the SM higgs loop given by Eq. (35) (orange line) for a better agreement, in particular for higher masses.

Next, we discuss the dependence of κ_λ on $s_{\beta-\alpha}$. We recall that $s_{\beta-\alpha} = 1$ implies that the lightest of the CP-even scalars in the 2HDM behaves precisely as the SM higgs. In order to remove the dependence of the BSM scalar loops, we choose as benchmark a degenerate scenario. As Fig. 2 shows, the inclusion of one loop corrections will decrease the value of κ_λ , and the sub-leading corrections are important (in particular related to the top loop) to obtain a better agreement to the full calculation. The difference is more

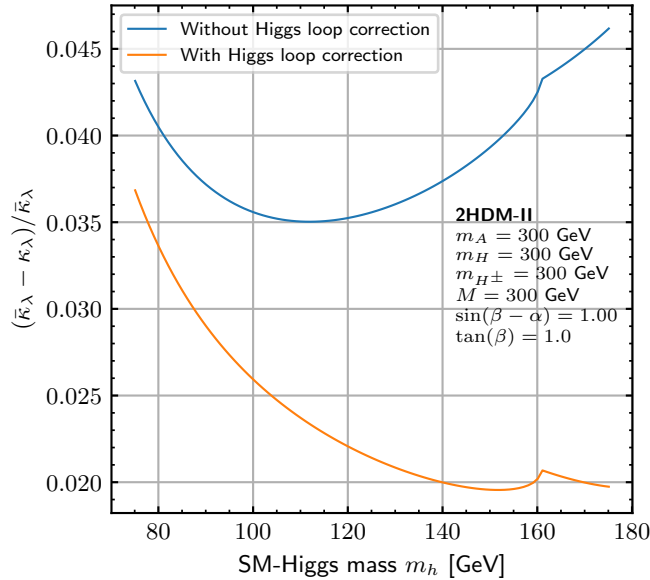


Figure 1. Deviation from the *anyH3* prediction, with and without including the Higgs loop, see Eq. (35). We choose the benchmark values shown in the figure, rendering contributions only from SM particles.

pronounced for values of $s_{\beta-\alpha} \sim 0.5$, which are disfavoured by present data from colliders [72]. In particular, the bound $s_{\beta-\alpha} > 0.995$ is enforced for type II 2HDM at 95% C.L. For this range, the leading contribution (including top and Higgs corrections) is at most 2% smaller than the full calculation.

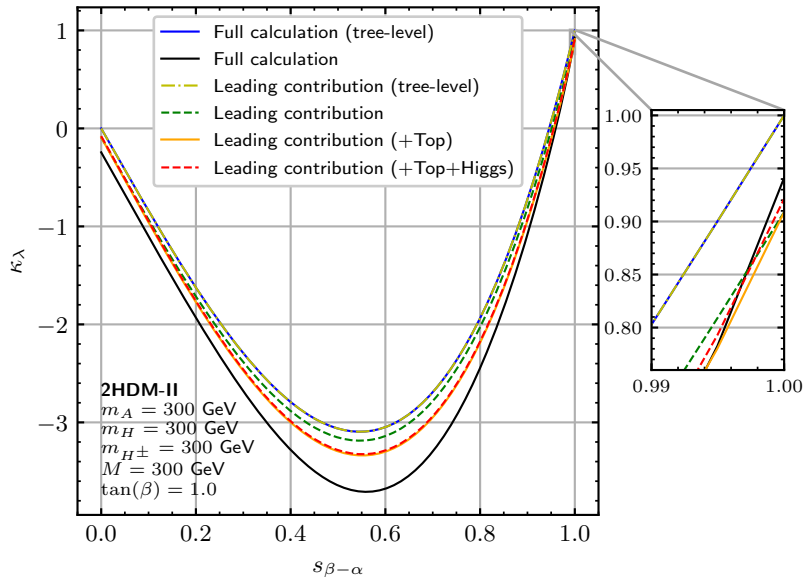


Figure 2. Dependence of κ_λ on $s_{\beta-\alpha}$ for the 2HDM type II. We choose the benchmark values showed in the figure. The black line is for the full calculation using *anyH3*, while the blue line is considering only the tree-level contribution. The light (dark) green line is considering tree (one-loop) contribution from Eq. (31), while the orange and red lines are including the top (subleading) and higgs loop corrections given by Eq. (35).

Next we discuss the influence of M on κ_λ , as shown in Fig. 3. We consider the alignment scenario for simplicity. At $M = 300$ GeV we recover the SM, for which $\kappa_\lambda < 1$ (recall that the top contribution is negative). As M increases, the corrections containing the BSM scalars all become negative as well, decreasing the value of κ_λ . We can, nevertheless,

single out only one of the BSM scalars contributions, by choosing degenerate masses and a suitable M as done in the left plot of Fig. 4. Notice that as m_A increases with **fixed** M , the value for κ_λ also increases, behaving roughly as $\kappa_\lambda \sim m_A^4(1 - 3M^2/m_A^2)$. On the other hand, for the 3-3-1 EFT, M is no longer a free parameter, implying that we can not remove the dependence on the other BSM scalar loops. Actually, the contribution from the loop containing the pseudoscalar A vanishes, see Eq. (39). Therefore, as m_A increases, as shown in the right plot of Fig. 4, κ_λ attains negative values.

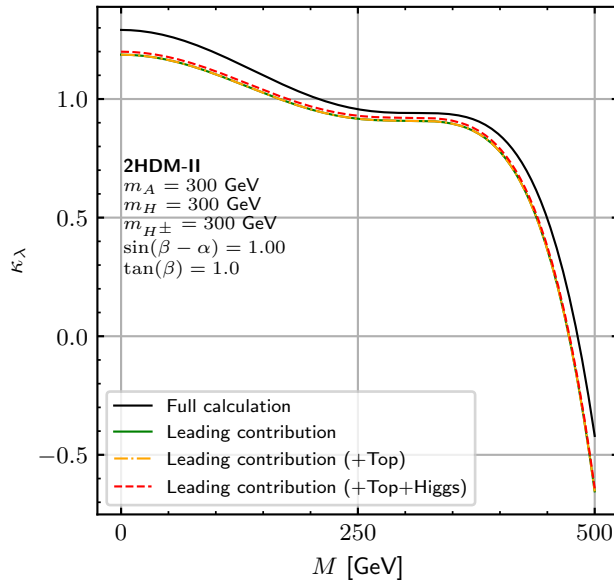


Figure 3. Dependence of κ_λ on M for the 2HDM type II. We choose the benchmark values showed in the figure. The black line is for the calculation using *anyH3*, the green line is considering Eq. (31), while the orange and red lines are including the top (subleading) and Higgs loop corrections given by Eq. (35).

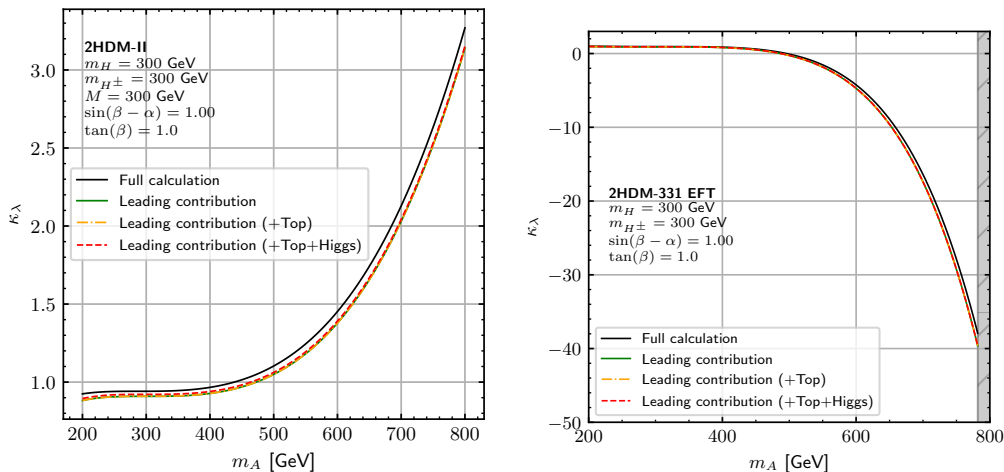


Figure 4. Dependence of κ_λ on M_A for the 2HDM type II (left) and the 3-3-1 EFT (right). We choose the benchmark values showed in the figure. The black line is for the calculation using *anyH3*, the green line is considering Eq. (33), while the orange and red lines are including the top (subleading) and Higgs loop corrections given by Eq. (35). The gray area shows the region excluded by the perturbative unitarity constraint.

Finally we discuss the influence of $\tan\beta$ on κ_λ in Fig. 5. Since the top Yukawa is already close to the perturbativity limit, the region with $t_\beta < 1$ is disfavoured. Therefore,

we will focus on $t_\beta > 1$. For this range, the influence from ζ_u is marginal, while terms proportional to t_β will be the leading ones, in particular for large values of this parameter. Notice also that, according to Eq. (39), the dependence on t_β only appears if one allows deviations from the alignment limit. For degenerate masses, in particular, only corrections proportional to x^3 survive. Once these terms are included, we find a good agreement with the full calculation (see the pink curve of Fig. 5.)

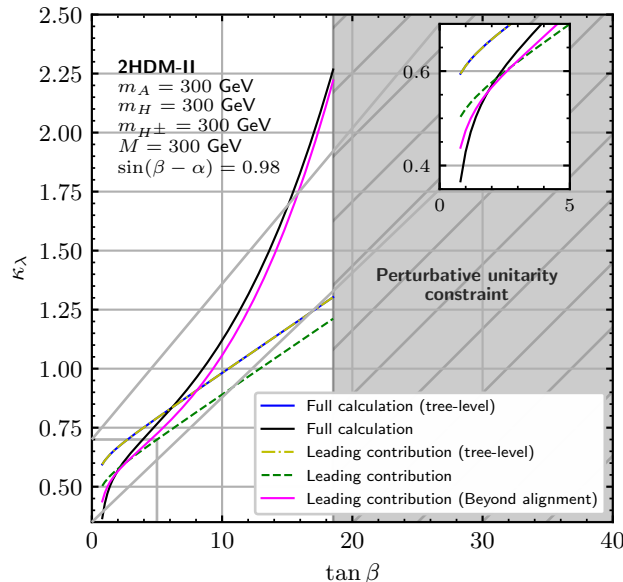


Figure 5. Dependence of κ_λ on $\tan\beta$ for the 2HDM type II. We choose the benchmark values showed in the figure. The black line is for the full calculation using *anyH3*, while the blue line is considering only the tree-level contribution. The light (dark) green line is considering tree (full) contribution from Eq. (33), while the pink line is including all refinements given in Eq. (39). The gray area shows the region excluded by the perturbative unitarity constraint.

To summarize, larger values for κ_λ are attained in the 3-3-1 EFT mostly by allowing a large split between the pseudo-scalar mass and the other BSM scalars masses. Large values for $\tan\beta$ can also play an important role, when one departs from the alignment limit.

We conclude this section briefly discussing the importance of two-loops corrections for κ_λ . As shown in [15], those can be relevant and even surpass the one-loop corrections. However, they are only known in the alignment regime [13, 14]. Since we aim to perform a comprehensive study of how large κ_λ can be in the 3-3-1 EFT, we opt to consider a non-alignment scenario in general, for which the two-loop corrections are not known. Thus we restrain our analysis for κ_λ at one-loop level. Nevertheless, in Appendix B we discuss how are findings for a alignment scenario would be impacted by the inclusion of two-loop corrections.

IV. PHENOMENOLOGY

Once we have established the most promising conditions to ensure a large κ_λ possibly detectable at the high luminosity regime of the LHC, we proceed to impose constraints from distinct sources on our model, including theoretical, flavor, and collider. We will describe each one of them in the following subsections. In order to assess the influence of those constraints in the multi-dimensional parameter space of our model, we will perform a scan on the mixing angle $s_{\beta-\alpha}$, the physical masses m_A , m_H , m_{H^\pm} , and t_β . For the 2HDM in general, we will also add M . We will adopt the following ranges as shown in Table I.

Parameter	$s_{\beta-\alpha}$	m_A (GeV)	m_H (GeV)	m_{H^\pm} (GeV)	t_β	M (GeV)
Range	(0.98 - 1)	(125 - 1500)	(125 - 1500)	(125 - 1500)	(0.8 - 40)	(100 - 5000)

Table I. Range of the free parameters used on the scan. When considering alignment, we do not allow $s_{\beta-\alpha}$ to vary freely, and when considering the 3-3-1 EFT, we do not vary M freely.

We scan the parameter space until around three to five thousand points pass all the imposed constraints. Then, after establishing the regions where the coupling is larger, we perform a dedicated scan up to, again, three to five thousand points in those regions to find the maximal value. Thus, we consider, in total, around 10 000 points of data in our scan that complies to every bound considered.

A. Theoretical

As customary in models with multiple scalars, we have to enforce the stability of scalar potential (bounded from below conditions), perturbative of its coupling as well as perturbative unitarity for the scattering matrix. As shown in [70], all these theoretical conditions, for the 3-3-1 EFT, can be extracted from the 2HDM [77, 78]. We have employed our own implementation for stability and perturbative conditions. For perturbative unitarity (PU) we relied on the implementation available at *anyBSM* [75], which computes the eigenvalue a_0 for the $SS \rightarrow SS$ scattering matrix for each of the scalars $S = A, H, H^\pm$ and automatically selects the maximum value. Since the PU bound will play a decisive role to constraint the parameter space of our model, we opted to show it as a separate constraint in our scan and we consider that $|\text{Re}(a_0)| < 0.5$. For the other two constraints, we will reserve the letters P for perturbativity of the quartic couplings (assumed to be smaller than 4π) and S for the stability of the scalar potential.

We show in Fig. 6 how the theoretical bounds limit the parameter space of the mass differences and the maximal value of κ_λ . Recall that, in the 3-3-1 EFT, $M = m_A$. Larger

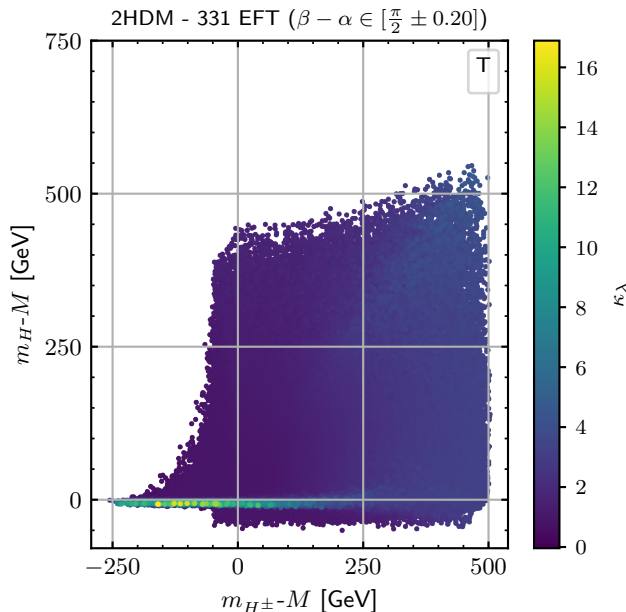


Figure 6. Parameter space of mass difference for points that comply with all theoretical bounds (perturbativity (P), stability (S) and unitarity (PU) = (T)) as function of the value of κ_λ .

values for κ_λ are attained in the region $m_{H^\pm}^\pm < m_A$ and $m_H \sim m_A$. As mentioned, the perturbative unitarity bound plays a critical role in constraining the parameter space for

critical values of κ_λ . In Fig. 7 (left) we show that PU forbids a large splitting between m_H and m_A . Moreover, it will be crucial to remove points with large t_β , as presented in Fig. 5. In Fig. 7 (right) we show how Fig. 6 would appear if PU were not enforced. It is possible to see that the perturbative unitarity bound restricts the maximal value of the trilinear Higgs coupling to less than half of the maximum allowed value from the other theoretical constraints, due to removing regions with large $\tan\beta$.

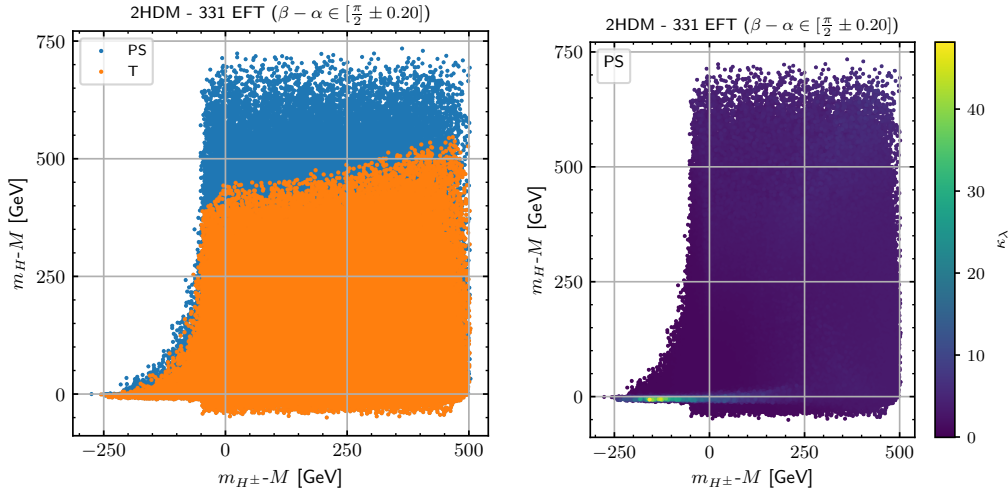


Figure 7. Parameter space of mass difference for points that comply with perturbativity (P) and vacuum stability (S) bounds as function of the value of κ_λ (left) and the comparison of the former case with the parameter space allowed region for all of the theoretical bounds (T), that is, including the perturbative unitarity bounds (PU) (right).

B. Electroweak constraints

We consider next the S, T, and U parameters. In 2022, the CDF collaboration released an updated value for the W-boson mass, which differ by more than 7σ from the SM prediction [79]. More recently, the ATLAS provided also a updated analysis, not finding significant deviation from previous measurements [80]. Until this tension is settled, we opt to consider two cases in the present work. In the first, we assume the values for S,T parameters (hereafter we assume $\Delta U = 0$) obtained by employing the reported W-mass from the ATLAS collaboration [81]

$$\Delta S = -0.05 \pm 0.07, \quad \Delta T = 0.00 \pm 0.06, \quad \text{correlation} = 0.93 \quad (40)$$

The second case is by considering only the CDF measurement for the W-mass [82]

$$\Delta S = 0.15 \pm 0.08, \quad \Delta T = 0.27 \pm 0.06, \quad \text{correlation} = 0.93 \quad (41)$$

For the evaluation of the S, T parameters, we employed *SPheno* [83, 84] within the 2HDM. For the 3-3-1 EFT, we considered further that $\lambda_5 \sim 0$. Since these parameters are obtained from radiative corrections, the heavy spectrum of the 3-3-1 model could play a role. We have explicitly checked that this is not the case, employing the formulas for the S, T parameter in the 3-3-1 model in general [85].

In Fig. 8, we show how the electroweak precision bounds (EW) constrain our main parameter space. All points comply with PS (from theoretical bounds). We note that EW is one of the main constraints for the parameter space, and it also helps to reduce the maximal value of κ_λ , despite not being the major factor (by comparison with the right figure in Fig. 7). In particular, it enforces either $m_{H^\pm} \sim m_A$ or $m_{H^\pm} \sim m_H$. In Fig. 9,

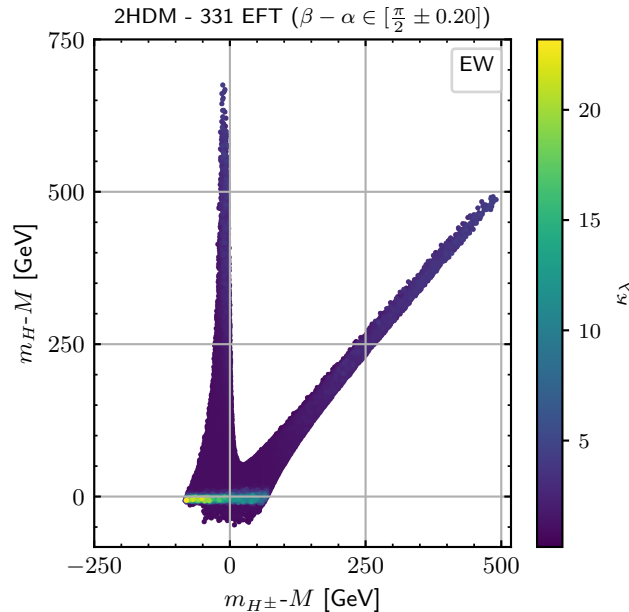


Figure 8. Parameter space of mass difference for points that comply with electroweak precision observable bounds (from PDG) as function of the value of κ_λ .

we show how the measurement from CDF for the W -mass changes the allowed parameter space region. We see that the maximum value of κ_λ in this case is slightly higher compared to the PDG value. We also show the comparison between the parameter space in each case and note that the regions are almost disjoint, as would be expected since the two results are in tension with one another.

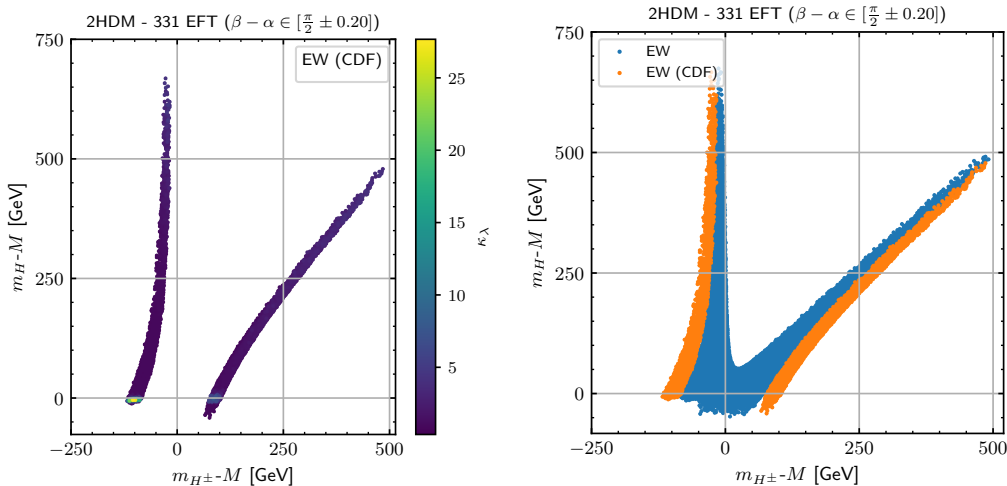


Figure 9. Parameter space of mass difference for points that comply with electroweak precision observable bounds (from CDF measurement) as function of the value of κ_λ (left) and the comparison of the former case with the parameter space allowed for the PDG global fit (as shown in Fig. 8) (right).

C. Collider

In order to systematically incorporate bounds coming from colliders into our numerical scan, we make use of *HiggsTools* [86–90], a successor to the two packages *HiggsSignals* and *HiggsBounds*. *HiggsSignals* is used to reinterpret the known 125 GeV-Higgs resonances

found in multiple channels, as well as its properties, in the case of extra scalar fields. Employing a χ^2 distribution, we quantify the agreement between the model predictions for given parameters with the available data, excluding points that do not fit the known resonances at 95% confidence level. With *HiggsBounds*, we also employ a χ^2 distribution to quantify the exclusion of given model parameters, based on direct searches at the LHC for scalar particle signals. *Higgsbounds* automatically selects the channel that provides the most stringent constraints, evaluating if such set of parameters is excluded or not at 95% confidence level. We find that the channels that are most constraining for the parameter space are $h, H \rightarrow ZZ \rightarrow 4\ell, 2\ell 2\nu$; $h \rightarrow \gamma\gamma, ZZ, WW, \tau\tau, bb$ [91–93]; $gg \rightarrow A \rightarrow Zh(\bar{b}b)$ [94]; $gg \rightarrow H, A \rightarrow \tau\tau(\bar{b}b)$ [95]; $A \rightarrow ZH \rightarrow \ell\ell WW, \ell\ell bb$ [96]; and $t \rightarrow bH^\pm \rightarrow b\tau^\pm\nu$ [97], but other channels were considered as well.

Among the previously considered channels, the scalar-vector and scalar-scalar couplings are mostly sensitive to deviations from the alignment situation. Specifically, the decay rates $h \rightarrow ZZ, \gamma\gamma, WW \propto s_{\beta\alpha}$, while $H \rightarrow ZZ, \gamma\gamma, WW$ and $A \rightarrow ZH$ are proportional to $c_{\beta-\alpha}$. Thus, when the alignment condition is met, we recover the SM case and the bounds are weaker. The scalar-fermionic couplings, on the other hand, are mostly proportional to t_β , so $h, H, A \rightarrow \tau\tau, bb$ give us the strongest constraints on $\tan\beta$ ³.

In Fig. 10 we show the influence of collider bounds on the parameter space of our model (to be compared with the right Fig. 7). Notice that the maximal value for κ_λ is drastically

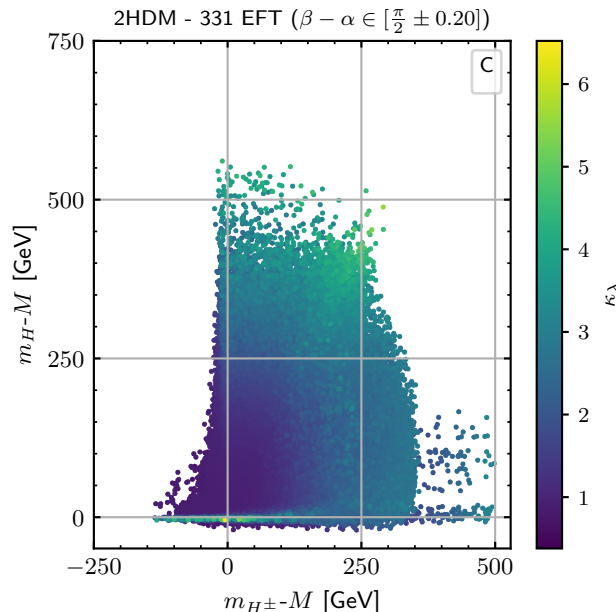


Figure 10. Parameter space of mass difference for points that comply with collider bounds as function of the value of κ_λ .

reduced, even though a relatively large splitting between the scalars is still allowed. The main reason behind this behavior is the constrain on the deviation from the alignment limit ($s_{\beta-\alpha}$) as well as the maximal value for t_β , as one can see in Fig. 11. In the left, we show every point in this parameter space that is allowed by perturbativity and vacuum stability, with its respective value of κ_λ . In the same plot, we show in red the approximate region containing the majority of points allowed by collider constraints. On the right, we show how all the bounds discussed so far constraint this parameter space and the maximal value of κ_λ . As we showed before, κ_λ increases with t_β , even for a mass degenerate scenario. However, this behavior is only possible if deviations from the alignment limit are enforced.

³ This is true mostly for Type II 2HDM, where the couplings to down-type quarks and leptons are proportional to $\tan\beta$ [71]. For Type I, it is still possible to impose such constraints but they will be significantly weaker.

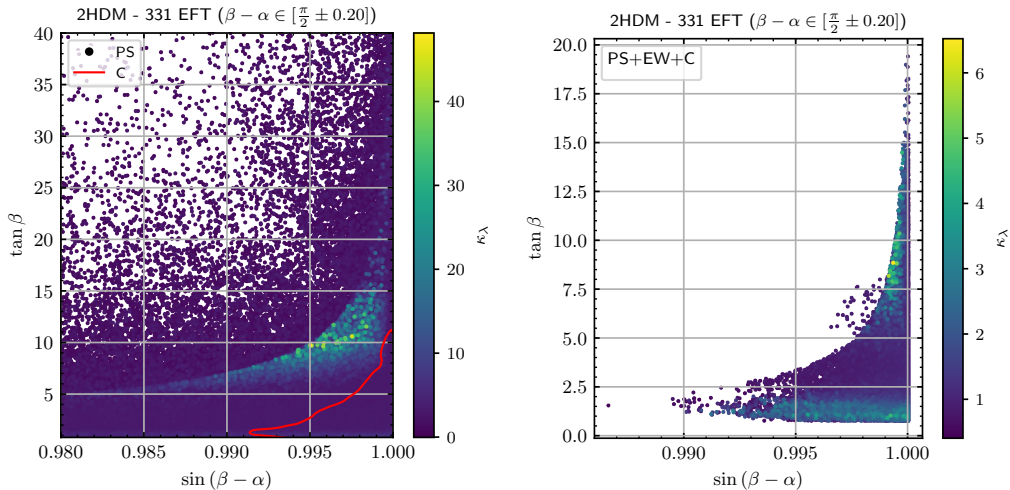


Figure 11. Parameter space of $\sin(\beta - \alpha)$ by $\tan\beta$ as a function of the value of κ_λ . On the left, we show all the points that pass the perturbativity and stability tests compared to the approximate region of the points that pass collider constraints (enclosed by the red curve). On the right, we show the points that pass all the bounds discussed so far.

In Fig. 11 one can see that collider bounds are very restrictive to $s_{\beta-\alpha}$, constraining it to the interval $[0.990, 1]$, as well as limiting the maximal value of $\tan\beta$, which is restricted to $\tan\beta < 20$.

D. $B \rightarrow X_s \gamma$

An stringent constraint for 2HDM in general is due to the decay $B \rightarrow X_s \gamma$, which agrees well with the SM prediction. This bound is particularly important for Type II, since there is an enhancement of the coupling between the charged scalar and the bottom quark given by t_β in this case. Using the analytic formulas of [98], one finds a lower bound on the charged scalar mass around 600 GeV, which is independent of the value of t_β . For the 3-3-1 EFT, one has more freedom when defining the Yukawa sector. In particular, this model allows a physical realization of the mixing matrices V_u , and V_d , as opposed to the SM (or 2HDM) where only their product $V_u^\dagger V_d$ is physical (parametrized as the CKM matrix). By adopting specific choices for V_u , it is possible to relax the constraint on the charged scalar mass [69, 70, 73]. In our work, however, in order to be conservative, we will adopt V_u as the identity matrix, which renders V_d as the CKM matrix. It is straightforward to implement the results of Ref. [98] for our model, rendering the allowed parameter space depicted in Fig. 12.

E. Maximal λ_{hhh} in the 3-3-1 EFT

To summarize, we obtain that by imposing only the theoretical bounds (PS) κ_λ can range up to 45, see Fig. 7. When constraints from flavor ($bs\gamma$) are also included, we still attain the same large value for κ_λ . However the available parameter space is significantly reduced, see Fig. 12. More importantly is the addition of electroweak precision observables (EW). It reduces κ_λ , which can be up to 25, as well as the available parameter space, see Fig. 8. Nevertheless, the main constraint is provided by collider searches (C), which renders κ_λ to be order of 6, see Fig. 10. In order to highlight the importance of the distinct constraints on restricting the parameter space, we show in Fig. 13 every set of bounds superposed.

The theoretical bounds (T), shown in blue, restrict m_{H^\pm} to be at most 500 GeV larger

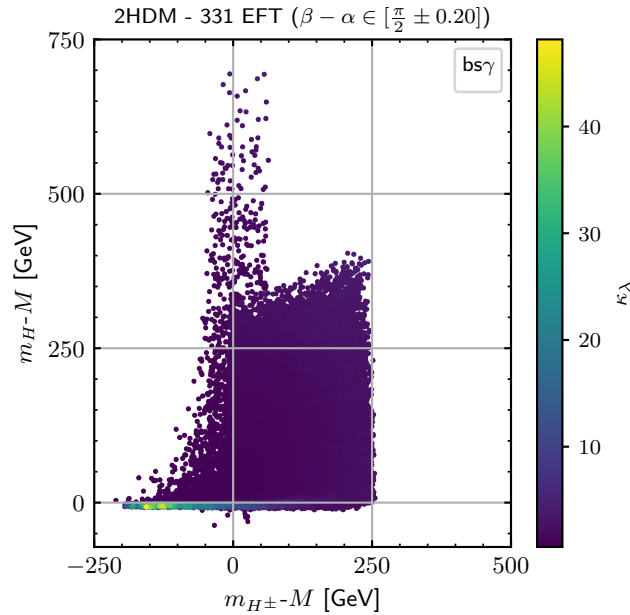


Figure 12. Parameter space of mass difference for points that comply with $b \rightarrow s\gamma$ present bounds, as a function of the value of κ_λ .

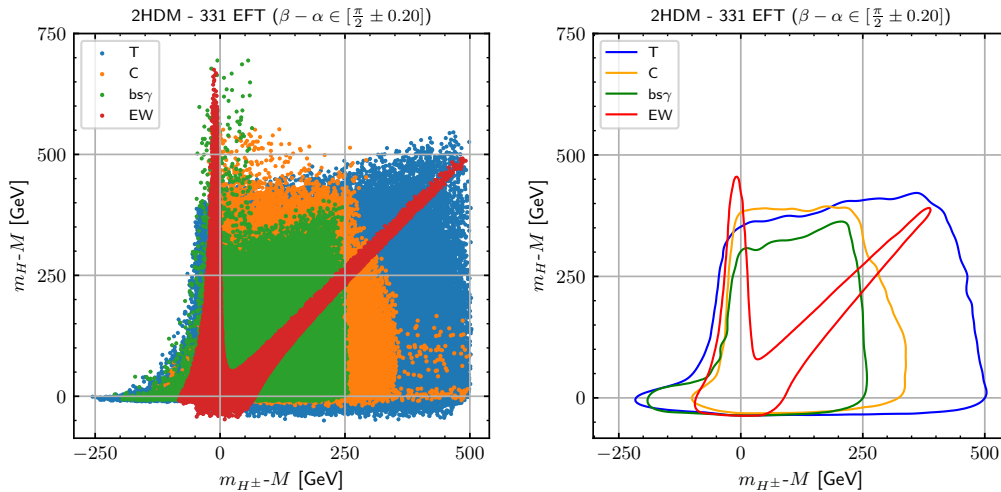


Figure 13. Comparison of points that comply with each set of bounds, theoretical (T), collider (C), flavor ($bs\gamma$), and electroweak precision observables (EW).

than m_A , while the splitting between m_H and m_A is generally a little smaller. Moreover, the region where A is the heaviest of the BSM scalars is significantly constrained. These findings, however, do not restrict much the maximal value of κ_λ , which can still be as large as 17. For the electroweak precision observables (EW), in red, we notice that they are important to restrict the splitting between the BSM scalars masses. In particular, it is not possible to have simultaneously m_H , and m_A far away from m_{H^\pm} . Regarding κ_λ , though, these constraints are weaker than T, as can be seen in Fig. 8, where κ_λ can be as large as 25. The $b \rightarrow s\gamma$ bound, in green, is very effective to reduce the splitting between m_{H^\pm} and m_A to be at most 250 GeV. It also restricts the splitting between m_H and m_A , but to a lesser extent. Regarding κ_λ , however, this bound alone still allowed for values as large as 25. Finally, it should be noticed that the allowed region after imposing collider bounds, in orange, is larger than the allowed region when considering $b \rightarrow s\gamma$. However, collider bounds are the most restrictive to the maximal value of κ_λ , by enforcing $s_{\beta-\alpha}$

to be close to one. As a result, the region with large $\tan\beta$ is also excluded, which was responsible for the largest values for κ_λ .

The final allowed region, which complies with all the bounds simultaneously, is shown in Fig. 14 (left). As anticipated, we observe larger values of κ_λ in the region where both m_H and m_{H^\pm} have a large splitting with M . At first glance, it is surprising to also see large values of κ_λ in the lower left part of the parameter space, that is, for $m_H \sim m_{H^\pm} \sim M$. As we show in Fig. 14 (right), this region is precisely where $\tan\beta$ is largest. To evidence the

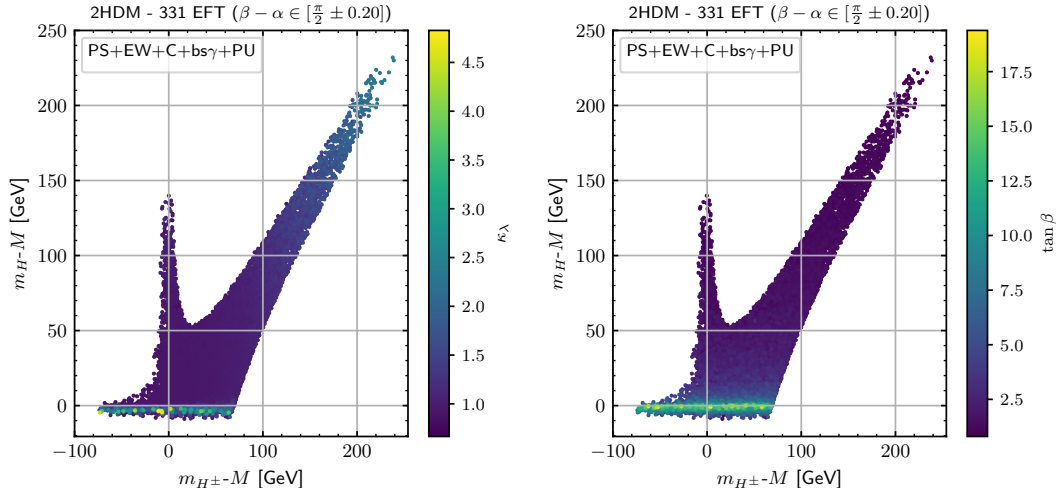


Figure 14. Parameter space of mass difference for points that comply with all bounds, as a function of the value of κ_λ (left) or $\tan\beta$ (right).

impact of the out-of-alignment condition on the maximal value of κ_λ , we show the same results but enforcing $s_{\beta-\alpha} = 1$ in Fig. 15. Note that the maximal value of κ_λ is reduced ⁴

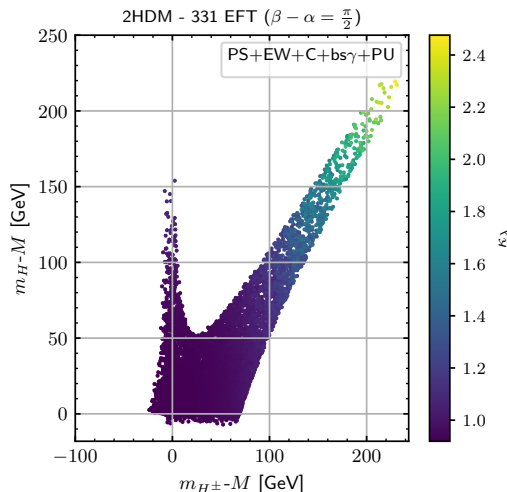


Figure 15. Parameter space of mass difference for points that comply with all bounds, imposing the alignment condition ($s_{\beta-\alpha} = 1$).

and now the region where $m_H \sim M$ no longer provides sizable values for the trilinear Higgs coupling. This shows that even with the very restrictive experimental constraints to $s_{\beta-\alpha}$, and thus, allowing only very small deviations to unity, it is possible to significantly increase the trilinear coupling in this situation. For completeness, we discuss in Appendix A the

⁴ When including two-loop corrections, which are known only at the alignment regime, it is still possible to attain values for $\kappa_\lambda \sim 3.5$. See Appendix B.

allowed region for a 2HDM Type I and II, as opposed to the 3-3-1 EFT considered in this work.

Now, if we instead consider the measurement from CDF for the W-mass, we assume that this measurement does not alter significantly other well-established parameters, namely the Fermi constant, the Yukawa couplings, and the SM vacuum expectation value. Therefore, the only significant impact of this is in the STU parameters, as already discussed. We, then, obtain the result shown in Fig. 16. We see that, even though the allowed region for

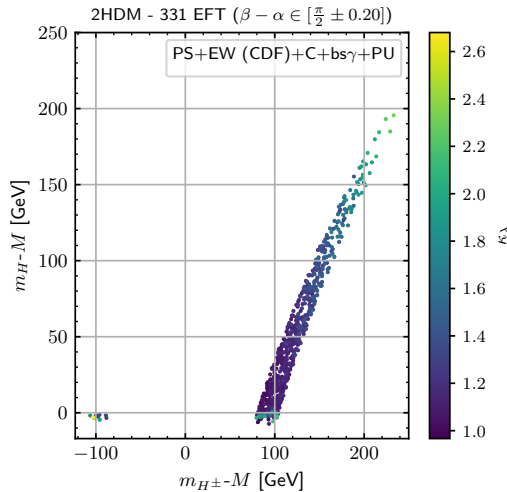


Figure 16. Parameter space of mass difference for points that comply with all bounds as function of the value of κ_λ . We, however, use the STU observables calculated using the CDF measurement of m_W , as opposed to the PDG combined fit.

the modified STU parameters considering the CDF measurement, shown in Fig. 9, allows a slightly bigger value of κ_λ compared to the PDG measurement, shown in Fig. 8, these bigger values of κ_λ vanish when other bounds are imposed, mostly collider bounds.

In conclusion, we find that combining all the most important constraints, there are two different conditions to maximize κ_λ in this model, a small mass splitting with a relatively large $\tan\beta$ (order of $\tan\beta \sim 10$), or with large mass splittings with M . The former condition is mostly restricted by collider searches and to a lesser degree by EW observables, yielding the largest value for κ_λ , while the latter is mostly restricted by PU, $bs\gamma$ and collider bounds.

Furthermore, with a maximal value of order 4.5, we conclude that this parameter space can be further constrained and explored with the next phase of the LHC, with a higher luminosity [5–7, 99] and also with the potential construction of the next-generation colliders, such as the Future Circular Collider (FCC) [100–102], for example.

V. CONCLUSIONS

We presented a general parameter scan of the low-energy limit of the 3-3-1 class of models. With the heavy degrees of freedom integrated out, we obtain an effective field theory (3-3-1 EFT) which can be mapped into a kind of 2HDM Type II in which terms of the general scalar potential of 2HDMs, namely (λ_5 , λ_6 and λ_7) are suppressed by v_{SM}/v_χ , where v_χ represents the heavy scale. The effective model also features a different structure for the Yukawa couplings among generations, however, by restricting to the third family, the couplings can be mapped to the 2HDM Type II exactly. Then, we perform a scan in the parameter space of the theory, imposing bounds of perturbativity, vacuum stability, perturbative unitarity, S , T , and U precision parameters at one-loop, collider known resonances and direct scalar searches, as well as $B \rightarrow X_s \gamma$ decay rate, evaluating

the potential impact of each of these bounds on the maximal value of the trilinear Higgs coupling. We find that the collider constraints are the most effective in limiting the value of κ_λ , mostly due to its impact on the bounds in $s_{\beta-\alpha}$, $\tan\beta$, and $m_\Phi - M$ ($\Phi = H, A, H^\pm$). The latter is already known in the literature to have an impact on κ_λ , however, it is typically considered, due to the experimental constraints, the alignment condition $s_{\beta-\alpha} = 1$, so that the former two are usually disregarded. In this work, we show that even for small deviations of the alignment condition, $s_{\beta-\alpha} \approx 0.995$, allowed by experiments, the impact of $s_{\beta-\alpha}$ and $\tan\beta$ can be significant, even generating the biggest values of κ_λ . We also present an approximate formula for κ_λ at one-loop, valid for the non-alignment scenario, which we confront with the full calculation, obtaining a good agreement. Finally, we get a maximal value of $\kappa_\lambda \approx 4.5$ for the 3-3-1 EFT, meaning that it is possible to explore this feature of the model in the next few years after the upcoming upgrades in the LHC and future colliders.

ACKNOWLEDGMENTS

A.L.C is supported by a postdoctoral fellowship from the Postdoctoral Researcher Program - Resolution GR/Unicamp No. 33/2023. LJFL is thankful for the support of CAPES under grant No. 88887.613742/2021-00.

Appendix A: Type I and Type II models

In this section, we aim to compare the different 2HDM types, more specifically the types I and II and the EFT arising from the 3-3-1 model. The same conclusions can be easily extended to the lepton-specific and flipped ones, since the Yukawa coupling to leptons do not play a significant role in this analysis. Therefore, we can immediately map the Lepton-Specific to Type I and the Flipped to Type II.

The results of our scan, for the alignment scenario, are shown in Figs. 17 and 18.

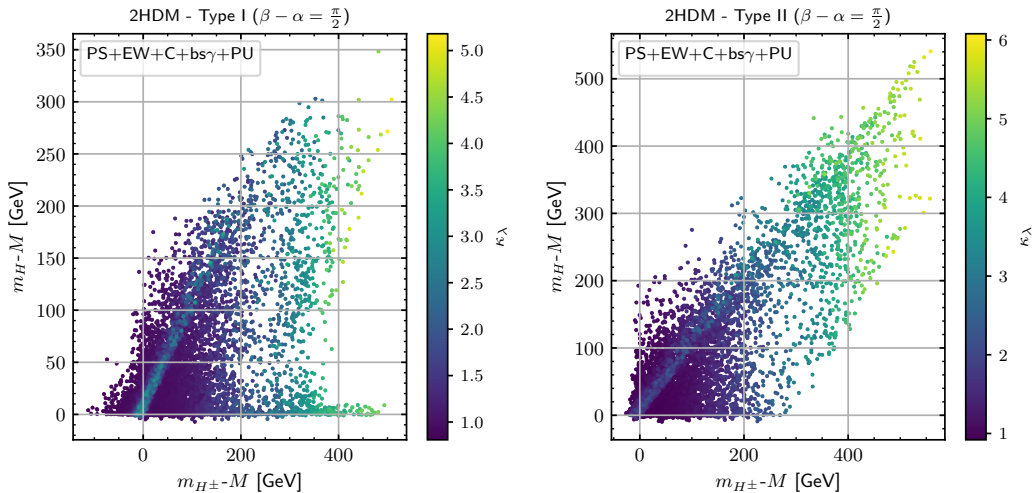


Figure 17. Parameter space of mass difference for points that comply with all bounds as function of the value of κ_λ for 2HDM types I (left) and II (right), under the alignment condition.

We find that, in the alignment limit, there is not a significant difference between Type I and Type II. The trilinear coupling can be slightly bigger for Type II, however, it is not possible to assert with certainty that this is not due to the finite amount of points considered in the scan.

Since these models, in general, have $\lambda_5 \neq 0$, they have one extra free parameter which can increase the value of κ_λ . Indeed, comparing to Fig. 15, it is noticeable that they allow

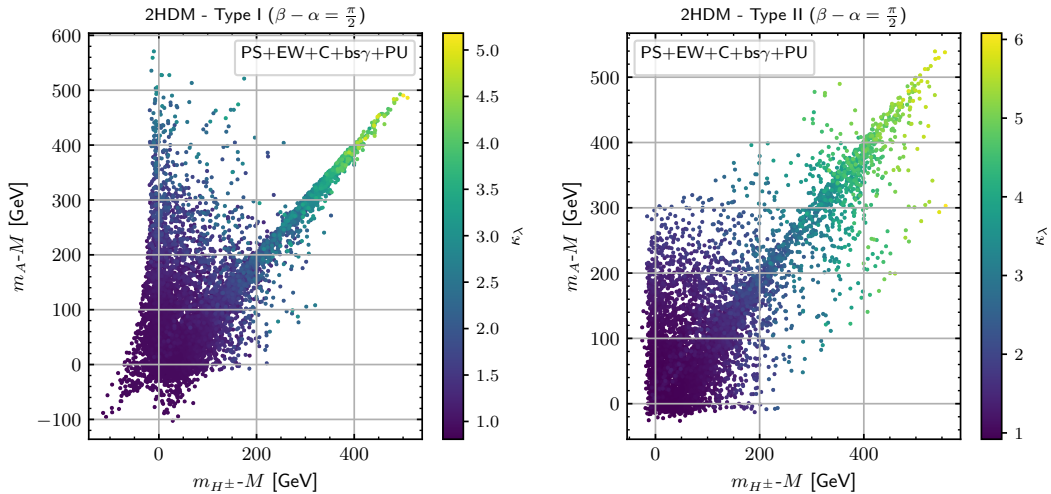


Figure 18. Parameter space of mass difference for points that comply with all bounds as function of the value of κ_λ for 2HDM types I (left) and II (right), under the alignment condition.

for bigger values of κ_λ when compared to the 3-3-1 EFT. This extra free-parameter, in the form of $m_A - M$ is shown in Fig. 18.

It is possible to see that a large splitting between m_A and M significantly increase the value of κ_λ , especially when such splitting also occurs for m_{H^\pm} . This gives this particular V-shape format in the parameter space of Fig. 18, where the “extremities of the V” reach the largest values of the trilinear coupling. On the other hand, from Fig. 17, it is possible to see that a large splitting of m_H from M while keeping m_A , m_{H^\pm} in the same scale of M is not attainable, nor there is a large impact of $m_H - M$ on the value of κ_λ , compared to the other splittings. Still, the conclusion is the same as before, the largest possible values for the trilinear coupling are obtained when $m_\phi \gg M$ and the physical masses are more or less in the same order of magnitude.

In Figs. 19 and 20 we show how this picture changes if the restriction on the alignment condition is lifted.

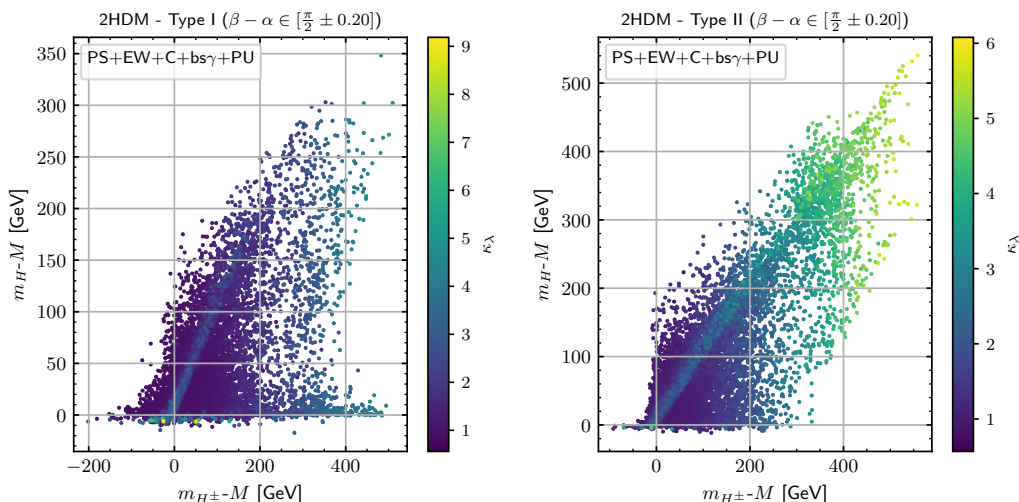


Figure 19. Parameter space of mass difference for points that comply with all bounds as function of the value of κ_λ for 2HDM types I (left) and II (right).

Comparing to Figs. 17 and 18, it is immediately evident that the maximal value of the trilinear coupling is around twice the maximum value when enforcing the alignment condition for Type I 2HDM. This is not unexpected, since it is well-known in the litera-

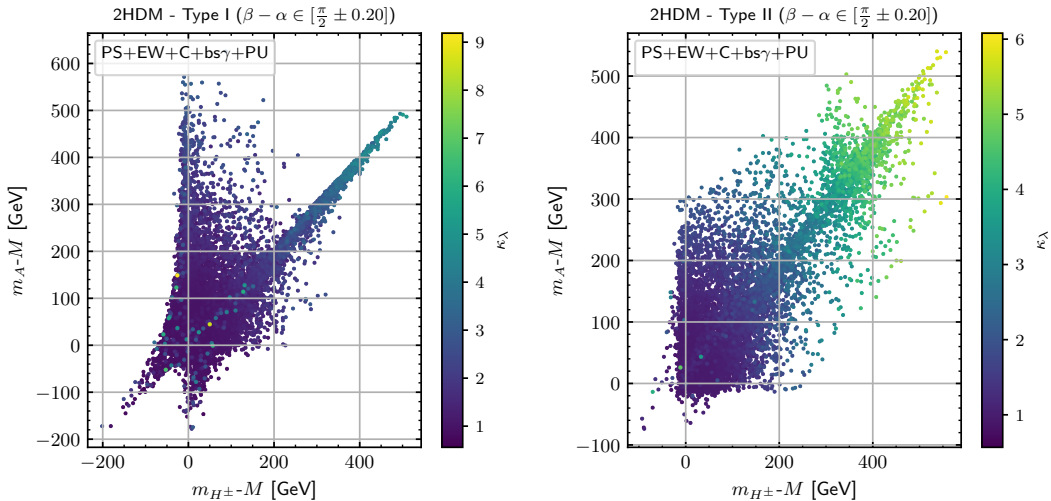


Figure 20. Parameter space of mass difference for points that comply with all bounds as function of the value of κ_{λ} for 2HDM types I (left) and II (right).

ture [72] that collider constraints are much more severe for Type II compared to Type I. Indeed, since slightly smaller $s_{\beta-\alpha}$ and larger values of $\tan\beta$ are allowed, the impact of these parameters can be more strongly seen in κ_{λ} .

Now, for Type II, compared to the 3-3-1 EFT in the alignment scenario (Fig. 15), one sees that the addition of M as a free parameter (Figs. 17 and 18) allows κ_{λ} to be twice as large. When one further considers out-of-alignment Type II (Figs. 19 and 20), the maximal value for the trilinear Higgs coupling is roughly the same. For the 3-3-1 EFT, on the other hand, lifting the restriction on the alignment condition allows significantly larger values for κ_{λ} (Fig. 14), of the order of the ones found in the Type II.

Appendix B: Two-loop calculation

In this section we discuss the influence of two-loop corrections for our findings. As already stated, those are known only for the alignment regime [13, 14]. In these references, κ_{λ} is expressed as

$$\kappa_{\lambda} = \kappa_{\lambda}^{(0)} + \left(\frac{1}{16\pi^2}\right) \kappa_{\lambda}^{(1)} + \left(\frac{1}{16\pi^2}\right)^2 \kappa_{\lambda}^{(2)} + \dots \quad (\text{B1})$$

The explicit formula for $\kappa_{\lambda}^{(2)}$ is given for the $\overline{\text{MS}}$ regularization scheme, together with all the ingredients to obtain $\kappa_{\lambda}^{(2)}$ at the on-shell (OS) scheme as well. Following the required steps, we obtained $\kappa_{\lambda}^{(2)}$ at the OS, and checked that the dependence on the regularization scale μ^2 cancel as expected.

Once $\kappa_{\lambda}^{(2)}$ is known at the OS scheme, we can study how our findings for the 3-3-1 EFT in the alignment scenario are modified. In order to make this comparison, we will define $\kappa_{\lambda}^{\text{NLO}}$ to be the trilinear higgs couplings modifier evaluated up to one-loop order, which we have considered in this manuscript up to this point. When two-loop corrections are also included, we obtain $\kappa_{\lambda}^{\text{NNLO}}$.

In Fig. 21 (left) we show the effect of including two-loop corrections for κ_{λ} . As can be easily seen, larger values are attained for $m_A \ll m_H \sim m_{H^{\pm}}$, which can reach up to 3.5. This should be compared against Fig. 15, where the same pattern emerges but κ_{λ} is at most 2.4. Thus, when including the two-loop corrections, one can obtain values up to 45% larger. We quantify this feature by showing in Fig. 21 (right) the ratio between the NNLO and NLO contributions. It should be noticed that not only the region $m_A \ll m_H \sim m_{H^{\pm}}$

allows the largest values for $\kappa_\lambda^{\text{NLO}}$, but it also maximizes the contribution from two-loop corrections.

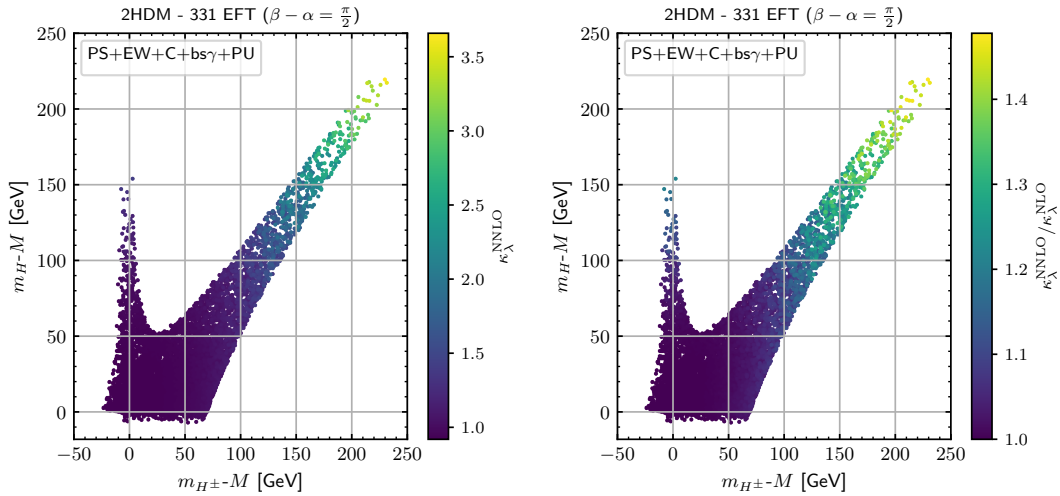


Figure 21. Parameter space of mass difference for points that comply with all bounds as function of the value of κ_λ at NNLO (left) and the ratio of NNLO by NLO (right) for 3-3-1 EFT.

We have also performed an analysis for the 2HDM Types I and II, findings similar results from [15].

-
- [1] **ATLAS Collaboration**, G. Aad *et al.*, *Observation of a new particle in the search for the Standard Model Higgs boson with the ATLAS detector at the LHC*, *Phys. Lett. B* **716** (2012) 1–29, [[1207.7214](#)].
 - [2] **CMS Collaboration**, S. Chatrchyan *et al.*, *Observation of a New Boson at a Mass of 125 GeV with the CMS Experiment at the LHC*, *Phys. Lett. B* **716** (2012) 30–61, [[1207.7235](#)].
 - [3] **ATLAS Collaboration**, G. Aad *et al.*, *A detailed map of Higgs boson interactions by the ATLAS experiment ten years after the discovery*, *Nature* **607** (2022), no. 7917 52–59, [[2207.00092](#)]. [Erratum: *Nature* 612, E24 (2022)].
 - [4] **CMS Collaboration**, A. Tumasyan *et al.*, *A portrait of the Higgs boson by the CMS experiment ten years after the discovery.*, *Nature* **607** (2022), no. 7917 60–68, [[2207.00043](#)]. [Erratum: *Nature* 623, (2023)].
 - [5] J. Chang, K. Cheung, J. S. Lee, and J. Park, *Probing the trilinear Higgs boson self-coupling at the high-luminosity LHC via multivariate analysis*, *Phys. Rev. D* **101** (2020), no. 1 016004, [[1908.00753](#)].
 - [6] M. Cepeda *et al.*, *Report from Working Group 2: Higgs Physics at the HL-LHC and HE-LHC*, *CERN Yellow Rep. Monogr.* **7** (2019) 221–584, [[1902.00134](#)].
 - [7] **ATLAS Collaboration**, *HL-LHC prospects for the measurement of Higgs boson pair production in the $b\bar{b}b\bar{b}$ final state and combination with the $b\bar{b}\gamma\gamma$ and $b\bar{b}\tau^+\tau^-$ final states at the ATLAS experiment*, .
 - [8] S. Kanemura, Y. Okada, and E. Senaha, *Electroweak baryogenesis and quantum corrections to the triple Higgs boson coupling*, *Phys. Lett. B* **606** (2005) 361–366, [[hep-ph/0411354](#)].
 - [9] T. Robens, T. Stefaniak, and J. Wittbrodt, *Two-real-scalar-singlet extension of the SM: LHC phenomenology and benchmark scenarios*, *Eur. Phys. J. C* **80** (2020), no. 2 151, [[1908.08554](#)].
 - [10] H. Abouabid, A. Arhrib, D. Azevedo, J. E. Falaki, P. M. Ferreira, M. Mühlleitner, and R. Santos, *Benchmarking di-Higgs production in various extended Higgs sector models*, *JHEP* **09** (2022) 011, [[2112.12515](#)].
 - [11] V. Brigljevic *et al.*, *HHH Whitepaper*, in *HHH Workshop*, 7, 2024. [2407.03015](#).
 - [12] S. Kanemura, Y. Okada, E. Senaha, and C. P. Yuan, *Higgs coupling constants as a probe of new physics*, *Phys. Rev. D* **70** (2004) 115002, [[hep-ph/0408364](#)].

- [13] J. Braathen and S. Kanemura, *On two-loop corrections to the Higgs trilinear coupling in models with extended scalar sectors*, *Phys. Lett. B* **796** (2019) 38–46, [[1903.05417](#)].
- [14] J. Braathen and S. Kanemura, *Leading two-loop corrections to the Higgs boson self-couplings in models with extended scalar sectors*, *Eur. Phys. J. C* **80** (2020), no. 3 227, [[1911.11507](#)].
- [15] H. Bahl, J. Braathen, and G. Weiglein, *New Constraints on Extended Higgs Sectors from the Trilinear Higgs Coupling*, *Phys. Rev. Lett.* **129** (2022), no. 23 231802, [[2202.03453](#)].
- [16] F. Pisano and V. Pleitez, *An $SU(3) \times U(1)$ model for electroweak interactions*, *Phys. Rev. D* **46** (1992) 410–417, [[hep-ph/9206242](#)].
- [17] P. H. Frampton, *Chiral dilepton model and the flavor question*, *Phys. Rev. Lett.* **69** (1992) 2889–2891.
- [18] J. C. Montero, C. A. de S. Pires, and V. Pleitez, *Neutrino masses through a type II seesaw mechanism at TeV scale*, *Phys. Lett. B* **502** (2001) 167–170, [[hep-ph/0011296](#)].
- [19] M. B. Tully and G. C. Joshi, *Generating neutrino mass in the 331 model*, *Phys. Rev. D* **64** (2001) 011301, [[hep-ph/0011172](#)].
- [20] J. C. Montero, C. A. De S. Pires, and V. Pleitez, *Neutrino masses through the seesaw mechanism in 3-3-1 models*, *Phys. Rev. D* **65** (2002) 095001, [[hep-ph/0112246](#)].
- [21] N. V. Cortez and M. D. Tonasse, *Calculable lepton masses, seesaw relations and four neutrino mixings in a 3-3-1 model with extra $U(1)$ symmetry*, *Phys. Rev. D* **72** (2005) 073005, [[hep-ph/0510143](#)].
- [22] D. Cogollo, H. Diniz, and C. A. de S. Pires, *KeV right-handed neutrinos from type II seesaw mechanism in a 3-3-1 model*, *Phys. Lett. B* **677** (2009), no. 5 338–342, [[0903.0370](#)].
- [23] D. Cogollo, H. Diniz, and C. A. de S. Pires, *Triple seesaw mechanism*, *Phys. Lett. B* **687** (2010) 400–404, [[1002.1944](#)].
- [24] D. Cogollo, H. Diniz, C. A. de S. Pires, and P. S. Rodrigues da Silva, *The Seesaw mechanism at TeV scale in the 3-3-1 model with right-handed neutrinos*, *Eur. Phys. J. C* **58** (2008) 455–461, [[0806.3087](#)].
- [25] A. G. Dias, C. A. de S. Pires, P. S. Rodrigues da Silva, and A. Sampieri, *A Simple Realization of the Inverse Seesaw Mechanism*, *Phys. Rev. D* **86** (2012) 035007, [[1206.2590](#)].
- [26] H. Okada, N. Okada, and Y. Orikasa, *Radiative seesaw mechanism in a minimal 3-3-1 model*, *Phys. Rev. D* **93** (2016), no. 7 073006, [[1504.01204](#)].
- [27] V. V. Vien, H. N. Long, and A. E. Cárcamo Hernández, *Lepton masses and mixings in a T' flavoured 3-3-1 model with type I and II seesaw mechanisms*, *Mod. Phys. Lett. A* **34** (2019), no. 01 1950005, [[1812.07263](#)].
- [28] T. P. Nguyen, T. T. Le, T. T. Hong, and L. T. Hue, *Decay of standard model-like Higgs boson $h \rightarrow \mu\tau$ in a 3-3-1 model with inverse seesaw neutrino masses*, *Phys. Rev. D* **97** (2018), no. 7 073003, [[1802.00429](#)].
- [29] C. A. de Sousa Pires, F. Ferreira De Freitas, J. Shu, L. Huang, and P. Wagner Vasconcelos Olegário, *Implementing the inverse type-II seesaw mechanism into the 3-3-1 model*, *Phys. Lett. B* **797** (2019) 134827, [[1812.10570](#)].
- [30] A. E. Cárcamo Hernández, N. A. Pérez-Julve, and Y. Hidalgo Velásquez, *Fermion masses and mixings and some phenomenological aspects of a 3-3-1 model with linear seesaw mechanism*, *Phys. Rev. D* **100** (2019), no. 9 095025, [[1907.13083](#)].
- [31] A. E. Cárcamo Hernández, Y. Hidalgo Velásquez, and N. A. Pérez-Julve, *A 3-3-1 model with low scale seesaw mechanisms*, *Eur. Phys. J. C* **79** (2019), no. 10 828, [[1905.02323](#)].
- [32] A. E. Cárcamo Hernández, L. T. Hue, S. Kovalenko, and H. N. Long, *An extended 3-3-1 model with two scalar triplets and linear seesaw mechanism*, *Eur. Phys. J. Plus* **136** (2021), no. 11 1158, [[2001.01748](#)].
- [33] T. T. Hong, L. T. T. Phuong, T. P. Nguyen, N. H. T. Nha, and L. T. Hue, *$(g-2)_{e,\mu}$ anomalies and decays $h, Z \rightarrow e\bar{e}\nu$ in 3-3-1 models with inverse seesaw neutrinos*, *Phys. Rev. D* **110** (2024), no. 7 075010, [[2404.05524](#)].
- [34] D. Fregolente and M. D. Tonasse, *Selfinteracting dark matter from an $SU(3)(L) \times U(1)(N)$ electroweak model*, *Phys. Lett. B* **555** (2003) 7–12, [[hep-ph/0209119](#)].
- [35] H. N. Long and N. Q. Lan, *Selfinteracting dark matter and Higgs bosons in the $SU(3)(C) \times SU(3)(L) \times U(1)(N)$ model with right-handed neutrinos*, *EPL* **64** (2003) 571, [[hep-ph/0309038](#)].
- [36] C. A. de S. Pires and P. S. Rodrigues da Silva, *Scalar Bilepton Dark Matter*, *JCAP* **12** (2007) 012, [[0710.2104](#)].
- [37] J. K. Mizukoshi, C. A. de S. Pires, F. S. Queiroz, and P. S. Rodrigues da Silva, *WIMPs in a 3-3-1 model with heavy Sterile neutrinos*, *Phys. Rev. D* **83** (2011) 065024, [[1010.4097](#)].
- [38] J. D. Ruiz-Alvarez, C. A. de S. Pires, F. S. Queiroz, D. Restrepo, and P. S. Rodrigues da

- Silva, *On the Connection of Gamma-Rays, Dark Matter and Higgs Searches at LHC*, *Phys. Rev. D* **86** (2012) 075011, [[1206.5779](#)].
- [39] S. Profumo and F. S. Queiroz, *Constraining the Z' mass in 331 models using direct dark matter detection*, *Eur. Phys. J. C* **74** (2014), no. 7 2960, [[1307.7802](#)].
- [40] P. V. Dong, T. P. Nguyen, and D. V. Soa, *3-3-1 model with inert scalar triplet*, *Phys. Rev. D* **88** (2013), no. 9 095014, [[1308.4097](#)].
- [41] P. V. Dong, H. T. Hung, and T. D. Tham, *3-3-1-1 model for dark matter*, *Phys. Rev. D* **87** (2013), no. 11 115003, [[1305.0369](#)].
- [42] D. Cogollo, A. X. Gonzalez-Morales, F. S. Queiroz, and P. R. Teles, *Excluding the Light Dark Matter Window of a 331 Model Using LHC and Direct Dark Matter Detection Data*, *JCAP* **11** (2014) 002, [[1402.3271](#)].
- [43] P. V. Dong, D. T. Huong, F. S. Queiroz, and N. T. Thuy, *Phenomenology of the 3-3-1-1 model*, *Phys. Rev. D* **90** (2014), no. 7 075021, [[1405.2591](#)].
- [44] P. V. Dong, N. T. K. Ngan, and D. V. Soa, *Simple 3-3-1 model and implication for dark matter*, *Phys. Rev. D* **90** (2014), no. 7 075019, [[1407.3839](#)].
- [45] C. Kelso, H. N. Long, R. Martinez, and F. S. Queiroz, *Connection of $g - 2_\mu$, electroweak, dark matter, and collider constraints on 331 models*, *Phys. Rev. D* **90** (2014), no. 11 113011, [[1408.6203](#)].
- [46] Y. Mambrini, S. Profumo, and F. S. Queiroz, *Dark Matter and Global Symmetries*, *Phys. Lett. B* **760** (2016) 807–815, [[1508.06635](#)].
- [47] P. V. Dong, C. S. Kim, D. V. Soa, and N. T. Thuy, *Investigation of Dark Matter in Minimal 3-3-1 Models*, *Phys. Rev. D* **91** (2015), no. 11 115019, [[1501.04385](#)].
- [48] C. A. de S. Pires, P. S. Rodrigues da Silva, A. C. O. Santos, and C. Siqueira, *Higgs mass and right-handed sneutrino WIMP in a supersymmetric 3-3-1 model*, *Phys. Rev. D* **94** (2016), no. 5 055014, [[1606.01853](#)].
- [49] A. Alves, G. Arcadi, P. V. Dong, L. Duarte, F. S. Queiroz, and J. W. F. Valle, *Matter-parity as a residual gauge symmetry: Probing a theory of cosmological dark matter*, *Phys. Lett. B* **772** (2017) 825–831, [[1612.04383](#)].
- [50] P. S. Rodrigues da Silva, *A Brief Review on WIMPs in 331 Electroweak Gauge Models*, *Phys. Int.* **7** (2016), no. 1 15–27, [[1412.8633](#)].
- [51] C. D. R. Carvajal, B. L. Sánchez-Vega, and O. Zapata, *Linking axionlike dark matter to neutrino masses*, *Phys. Rev. D* **96** (2017), no. 11 115035, [[1704.08340](#)].
- [52] P. V. Dong, D. T. Huong, F. S. Queiroz, J. W. F. Valle, and C. A. Vaquera-Araujo, *The Dark Side of Flipped Trinification*, *JHEP* **04** (2018) 143, [[1710.06951](#)].
- [53] G. Arcadi, C. P. Ferreira, F. Goertz, M. M. Guzzo, F. S. Queiroz, and A. C. O. Santos, *Lepton Flavor Violation Induced by Dark Matter*, *Phys. Rev. D* **97** (2018), no. 7 075022, [[1712.02373](#)].
- [54] J. C. Montero, A. Romero, and B. L. Sánchez-Vega, *Axion dark matter in a 3 – 3 – 1 model*, *Phys. Rev. D* **97** (2018), no. 6 063015, [[1709.04535](#)].
- [55] D. T. Huong, D. N. Dinh, L. D. Thien, and P. Van Dong, *Dark matter and flavor changing in the flipped 3-3-1 model*, *JHEP* **08** (2019) 051, [[1906.05240](#)].
- [56] C. E. Alvarez-Salazar and O. L. G. Peres, *Constraining the 3 – 3 – 1 model with heavy neutral leptons using $(g - 2)_\mu$ and dark matter observables*, *Phys. Rev. D* **103** (2021), no. 3 035029, [[1906.06444](#)].
- [57] D. Van Loi, C. H. Nam, and P. Van Dong, *Dark matter in the fully flipped 3-3-1-1 model*, *Eur. Phys. J. C* **81** (2021), no. 7 591, [[2012.10979](#)].
- [58] M. Dutra, V. Oliveira, C. A. de S. Pires, and F. S. Queiroz, *A model for mixed warm and hot right-handed neutrino dark matter*, *JHEP* **10** (2021) 005, [[2104.14542](#)].
- [59] V. Oliveira and C. A. de S. Pires, *PandaX-4T limits on Z' mass in 3-3-1LHN model*, *Phys. Rev. D* **106** (2022), no. 1 015031, [[2112.03963](#)].
- [60] M. M. Guzzo, L. J. F. Leite, and S. W. P. Novelo, *Neutrinos in a Minimal 3-3-1 Model*, *Front. in Phys.* **10** (2022) 812921.
- [61] P. B. Pal, *The Strong CP question in $SU(3)(C) \times SU(3)(L) \times U(1)(N)$ models*, *Phys. Rev. D* **52** (1995) 1659–1662, [[hep-ph/9411406](#)].
- [62] A. G. Dias and V. Pleitez, *Stabilizing the invisible axion in 3-3-1 models*, *Phys. Rev. D* **69** (2004) 077702, [[hep-ph/0308037](#)].
- [63] A. G. Dias, C. A. de S. Pires, and P. S. Rodrigues da Silva, *Discrete symmetries, invisible axion and lepton number symmetry in an economic 3 3 1 model*, *Phys. Rev. D* **68** (2003) 115009, [[hep-ph/0309058](#)].
- [64] J. C. Montero and B. L. Sanchez-Vega, *Natural PQ symmetry in the 3-3-1 model with a minimal scalar sector*, *Phys. Rev. D* **84** (2011) 055019, [[1102.5374](#)].

- [65] A. G. Dias, J. Leite, D. D. Lopes, and C. C. Nishi, *Fermion Mass Hierarchy and Double Seesaw Mechanism in a 3-3-1 Model with an Axion*, *Phys. Rev. D* **98** (2018), no. 11 115017, [[1810.01893](#)].
- [66] A. G. Dias, J. Leite, J. W. F. Valle, and C. A. Vaquera-Araujo, *Reloading the axion in a 3-3-1 setup*, *Phys. Lett. B* **810** (2020) 135829, [[2008.10650](#)].
- [67] A. Alves, L. Duarte, S. Kovalenko, Y. M. Oviedo-Torres, F. S. Queiroz, and Y. S. Villamizar, *Constraining 3-3-1 models at the LHC and future hadron colliders*, *Phys. Rev. D* **106** (2022), no. 5 055027, [[2203.02520](#)].
- [68] H. Okada, N. Okada, Y. Orikasa, and K. Yagyu, *Higgs phenomenology in the minimal $SU(3)_L \times U(1)_X$ model*, *Phys. Rev. D* **94** (2016), no. 1 015002, [[1604.01948](#)].
- [69] Z. Fan and K. Yagyu, *CP-violating 2HDMs emerging from 3-3-1 models*, *JHEP* **06** (2022) 014, [[2201.11277](#)].
- [70] A. L. Cherchiglia and O. L. G. Peres, *On the viability of a light scalar spectrum for 3-3-1 models*, *JHEP* **04** (2023) 017, [[2209.12063](#)].
- [71] G. C. Branco, P. M. Ferreira, L. Lavoura, M. N. Rebelo, M. Sher, and J. P. Silva, *Theory and phenomenology of two-Higgs-doublet models*, *Phys. Rept.* **516** (2012) 1–102, [[1106.0034](#)].
- [72] **ATLAS Collaboration**, G. Aad *et al.*, *Interpretations of the ATLAS measurements of Higgs boson production and decay rates and differential cross-sections in pp collisions at $\sqrt{s} = 13$ TeV*, [2402.05742](#).
- [73] A. Doff, J. P. Pinheiro, and C. A. d. S. Pires, *Exploring solutions to the muon $g-2$ anomaly in a THDM-like model under flavor constraints*, [2405.05839](#).
- [74] S. Kanemura, S. Kiyoura, Y. Okada, E. Senaha, and C. P. Yuan, *New physics effect on the Higgs selfcoupling*, *Phys. Lett. B* **558** (2003) 157–164, [[hep-ph/0211308](#)].
- [75] H. Bahl, J. Braathen, M. Gabelmann, and G. Weiglein, *anyH3: precise predictions for the trilinear Higgs coupling in the Standard Model and beyond*, *Eur. Phys. J. C* **83** (2023), no. 12 1156, [[2305.03015](#)]. [Erratum: *Eur.Phys.J.C* 84, 498 (2024)].
- [76] E. Senaha, *Radiative Corrections to Triple Higgs Coupling and Electroweak Phase Transition: Beyond One-loop Analysis*, *Phys. Rev. D* **100** (2019), no. 5 055034, [[1811.00336](#)].
- [77] M. Maniatis, A. von Manteuffel, O. Nachtmann, and F. Nagel, *Stability and symmetry breaking in the general two-Higgs-doublet model*, *Eur. Phys. J. C* **48** (2006) 805–823, [[hep-ph/0605184](#)].
- [78] I. F. Ginzburg and I. P. Ivanov, *Tree-level unitarity constraints in the most general 2HDM*, *Phys. Rev. D* **72** (2005) 115010, [[hep-ph/0508020](#)].
- [79] **CDF Collaboration**, T. Aaltonen *et al.*, *High-precision measurement of the W boson mass with the CDF II detector*, *Science* **376** (2022), no. 6589 170–176.
- [80] **ATLAS Collaboration**, G. Aad *et al.*, *Measurement of the W-boson mass and width with the ATLAS detector using proton-proton collisions at $\sqrt{s} = 7$ TeV*, [2403.15085](#).
- [81] **Particle Data Group Collaboration**, S. Navas *et al.*, *Review of particle physics*, *Phys. Rev. D* **110** (2024), no. 3 030001.
- [82] C.-T. Lu, L. Wu, Y. Wu, and B. Zhu, *Electroweak precision fit and new physics in light of the W boson mass*, *Phys. Rev. D* **106** (2022), no. 3 035034, [[2204.03796](#)].
- [83] W. Porod, *SPheno, a program for calculating supersymmetric spectra, SUSY particle decays and SUSY particle production at e^+e^- colliders*, *Comput. Phys. Commun.* **153** (2003) 275–315, [[hep-ph/0301101](#)].
- [84] W. Porod and F. Staub, *SPheno 3.1: Extensions including flavour, CP-phases and models beyond the MSSM*, *Comput. Phys. Commun.* **183** (2012) 2458–2469, [[1104.1573](#)].
- [85] J. T. Liu and D. Ng, *Z - Z-prime mixing and oblique corrections in an $SU(3) \times U(1)$ model*, *Z. Phys. C* **62** (1994) 693–700, [[hep-ph/9302271](#)].
- [86] H. Bahl, T. Biekötter, S. Heinemeyer, C. Li, S. Paasch, G. Weiglein, and J. Wittbrodt, *HiggsTools: BSM scalar phenomenology with new versions of HiggsBounds and HiggsSignals*, *Comput. Phys. Commun.* **291** (2023) 108803, [[2210.09332](#)].
- [87] P. Bechtle, O. Brein, S. Heinemeyer, O. Stål, T. Stefaniak, G. Weiglein, and K. E. Williams, *HiggsBounds – 4: Improved Tests of Extended Higgs Sectors against Exclusion Bounds from LEP, the Tevatron and the LHC*, *Eur. Phys. J. C* **74** (2014), no. 3 2693, [[1311.0055](#)].
- [88] P. Bechtle, D. Dercks, S. Heinemeyer, T. Klingl, T. Stefaniak, G. Weiglein, and J. Wittbrodt, *HiggsBounds-5: Testing Higgs Sectors in the LHC 13 TeV Era*, *Eur. Phys. J. C* **80** (2020), no. 12 1211, [[2006.06007](#)].
- [89] P. Bechtle, S. Heinemeyer, O. Stål, T. Stefaniak, and G. Weiglein, *HiggsSignals: Confronting arbitrary Higgs sectors with measurements at the Tevatron and the LHC*, *Eur.*

- Phys. J. C* **74** (2014), no. 2 2711, [[1305.1933](#)].
- [90] P. Bechtle, S. Heinemeyer, T. Klingl, T. Stefaniak, G. Weiglein, and J. Wittbrodt, *HiggsSignals-2: Probing new physics with precision Higgs measurements in the LHC 13 TeV era*, *Eur. Phys. J. C* **81** (2021), no. 2 145, [[2012.09197](#)].
- [91] **CMS Collaboration**, S. Chatrchyan *et al.*, *Measurement of the Properties of a Higgs Boson in the Four-Lepton Final State*, *Phys. Rev. D* **89** (2014), no. 9 092007, [[1312.5353](#)].
- [92] **CMS Collaboration**, *Combination of standard model Higgs boson searches and measurements of the properties of the new boson with a mass near 125 GeV*, .
- [93] **ATLAS Collaboration**, G. Aad *et al.*, *Search for heavy resonances decaying into a pair of Z bosons in the $\ell^+\ell^-\ell'^+\ell'^-$ and $\ell^+\ell^-\nu\bar{\nu}$ final states using 139 fb $^{-1}$ of proton–proton collisions at $\sqrt{s} = 13$ TeV with the ATLAS detector*, *Eur. Phys. J. C* **81** (2021), no. 4 332, [[2009.14791](#)].
- [94] **CMS Collaboration**, A. M. Sirunyan *et al.*, *Search for a heavy pseudoscalar boson decaying to a Z and a Higgs boson at $\sqrt{s} = 13$ TeV*, *Eur. Phys. J. C* **79** (2019), no. 7 564, [[1903.00941](#)].
- [95] **CMS Collaboration**, A. Tumasyan *et al.*, *Searches for additional Higgs bosons and for vector leptoquarks in $\tau\tau$ final states in proton-proton collisions at $\sqrt{s} = 13$ TeV*, *JHEP* **07** (2023) 073, [[2208.02717](#)].
- [96] **ATLAS Collaboration**, G. Aad *et al.*, *Search for a heavy Higgs boson decaying into a Z boson and another heavy Higgs boson in the $\ell\ell b\bar{b}$ and $\ell\ell WW$ final states in pp collisions at $\sqrt{s} = 13$ TeV with the ATLAS detector*, *Eur. Phys. J. C* **81** (2021), no. 5 396, [[2011.05639](#)].
- [97] **ATLAS Collaboration**, M. Aaboud *et al.*, *Search for charged Higgs bosons decaying via $H^\pm \rightarrow \tau^\pm\nu_\tau$ in the τ +jets and τ +lepton final states with 36 fb $^{-1}$ of pp collision data recorded at $\sqrt{s} = 13$ TeV with the ATLAS experiment*, *JHEP* **09** (2018) 139, [[1807.07915](#)].
- [98] T. Enomoto and R. Watanabe, *Flavor constraints on the Two Higgs Doublet Models of Z_2 symmetric and aligned types*, *JHEP* **05** (2016) 002, [[1511.05066](#)].
- [99] F. Gianotti *et al.*, *Physics potential and experimental challenges of the LHC luminosity upgrade*, *Eur. Phys. J. C* **39** (2005) 293–333, [[hep-ph/0204087](#)].
- [100] N. Arkani-Hamed, T. Han, M. Mangano, and L.-T. Wang, *Physics opportunities of a 100 TeV proton–proton collider*, *Phys. Rept.* **652** (2016) 1–49, [[1511.06495](#)].
- [101] J. Baglio, A. Djouadi, and J. Quevillon, *Prospects for Higgs physics at energies up to 100 TeV*, *Rept. Prog. Phys.* **79** (2016), no. 11 116201, [[1511.07853](#)].
- [102] R. Contino *et al.*, *Physics at a 100 TeV pp collider: Higgs and EW symmetry breaking studies*, [1606.09408](#).